Experimental Case Studies for Uncertainty Quantification in Structural Dynamics: Part 1, Beam Experiment

S. Adhikari [a,*,1]

[a] *School of Engineering, University of Wales Swansea, Singleton Park, Swansea SA2 8PP, United Kingdom*

M. I. Friswell [b,2]

[b] *Department of Aerospace Engineering, University of Bristol Queens Building, University Walk, Bristol BS8 1TR, United Kingdom*

K. Lonkar [c,3]

[c] *Department of Aerospace Engineering, Indian Institute of Technology, Kanpur, India*

Abstract

The consideration of uncertainties in numerical models to obtain the probabilistic descriptions of vibration response is becoming more desirable for industrial scale finite element models. Broadly speaking, there are two aspects to this problem. The first is the quantification of parametric and non-parametric uncertainties associated with the model and the second is the propagation of uncertainties through the model. While the methods of uncertainty propagation have been extensively researched in the past three decades (e.g., the stochastic finite element method), only relatively recently has quantification been considered seriously. This paper considers uncertainty quantification with the aim of gaining more insight into the nature of uncertainties in medium and high frequency vibration problems. This paper and its companion [1] describe in detail the setup and results from two experimental studies that may be used for this purpose. The experimental work in this paper uses a fixed-fixed beam with 12 masses placed at random locations. The total 'random mass' is about 2% of the total mass of the beam and this experiment simulates 'random errors' in the mass matrix. One hundred nominally identical dynamical systems are created and individually tested. The probabilistic characteristics of the frequency response functions are discussed in the low, medium and high frequency ranges. The variability in the amplitude and phase of the measured frequency response functions is compared with numerical Monte Carlo simulation results. The data obtained in this experiments may be useful for the validation of uncertainty quantification and propagation methods in structural dynamics.

Key words: Experimental modal analysis, stochastic dynamical systems, uncertainty quantification, model validation, beam experiment

Contents

1 Introduction

The steady development of powerful computational hardware in recent years has led to high-resolution finite element models of real-life engineering structural systems. However, for high-fidelity and credible numerical models, a high resolution in the numerical mesh is not enough. It is also required to quantify the uncertainties and robustness associated with a numerical model. As a result, the quantification of uncertainties plays a key role in establishing the credibility of a numerical model. Uncertainties can be broadly divided into two categories. The first type is due to the inherent variability in the system parameters, for example, different cars manufactured from a single production line are not exactly the same. This type of uncertainty is often referred to as *aleatoric uncertainty*. If enough samples are present, it is possible to characterize the variability using well established statistical methods and consequently the probably density functions (pdf) of the parameters can be obtained. The second type of uncertainty is due to the lack of knowledge regarding a system, often referred to as *epistemic uncertainty*. This kind of uncertainty generally arises in the modelling of complex

* Corresponding author, Tel: + 44 (0)1792 602088, Fax: + 44 (0)1792 295676
Email addresses: S.Adhikari@swansea.ac.uk (S. Adhikari), M.I.Friswell@bristol.ac.uk (M. I. Friswell), kuldeepl@iitk.ac.in (K. Lonkar).
URLs: http://engweb.swan.ac.uk/∼adhikaris (S. Adhikari), http://www.aer.bris.ac.uk/contact/academic/friswell/home_page.html (M. I. Friswell), http://home.iitk.ac.in/ kuldeepl/ (K. Lonkar).
[1] Chair of Aerospace Engineering
[2] Sir George White Professor
[3] Student

systems, for example, in the modelling of cabin noise in helicopters. Due to its very nature, it is comparatively difficult to quantify or model this type of uncertainty. There are two broad approaches to quantify uncertainties in a model. The first is the *parametric approach* and the second is the *non-parametric approach*. In the parametric approach the uncertainties associated with the system parameters, such as Young's modulus, mass density, Poisson's ratio, damping coefficient and geometric parameters, are quantified using statistical methods and propagated, for example, using the stochastic finite element method [2–10]. This type of approach is suitable to quantify aleatoric uncertainties. Epistemic uncertainty on the other hand does not explicitly depend on the system parameters. For example, there can be unquantified errors associated with the equation of motion (linear or non-linear), in the damping model (viscous or non-viscous), in the model of structural joints, and also in the numerical methods (e.g, discretisation of displacement fields, truncation and round-off errors, tolerances in the optimization and iterative algorithms, step-sizes in the time-integration methods). It is evident that the parametric approach is not suitable to quantify this type of uncertainty. As a result non-parametric approaches [11–13] have been proposed for this purpose.

Uncertainties associated with a variable can be characterized using the probabilistic approach or possibilistic approaches based on interval algebra, convex sets or Fuzzy sets. In this paper the probabilistic approach has been adopted. The equation of motion of a damped n-degree-of-freedom linear structural dynamic system can be expressed as

$$\mathbf{M}\ddot{\mathbf{q}}(t) + \mathbf{C}\dot{\mathbf{q}}(t) + \mathbf{K}\mathbf{q}(t) = \mathbf{f}(t) \tag{1}$$

where $\mathbf{M} \in \mathbb{R}_{n,n}$, $\mathbf{C} \in \mathbb{R}_{n,n}$ and $\mathbf{K} \in \mathbb{R}_{n,n}$ are the mass, damping and stiffness matrices respectively. The importance of considering parametric and/or non-parametric uncertainty also depends on the frequency of excitation. For example, in high frequency vibration the wave lengths of the vibration modes become very small. As a result the vibration response can be very sensitive to the small details of the system. In such situations a non-parametric uncertainty model may be adequate. Overall, three *different* approaches are currently available to analyze stochastic structural dynamic systems across the frequency range:

- *Low frequency vibration problems*: Stochastic Finite Element Method [2–10, 14] (SFEM) - considers parametric uncertainties in detail;
- *High frequency vibration problems*: Statistical Energy Analysis [15–17] (SEA) - does not consider parametric uncertainties in detail;
- *Mid-frequency vibration problems* [18–21]: both parametric and non-parametric uncertainties need to be considered.

The majority of the studies reported in probabilistic mechanics are based on analytical or simulation methods. Often simulation based methods are used to validate approximate but

relatively fast prediction tools (such as perturbation based methods). Experimental results are rare because of difficulties such as (a) generating nominally identical samples of a structural system, (b) the resources and effort involved in testing a large number of samples, (c) the repetitive nature of the experimental procedure and (d) ensuring that different samples are tested in exactly the same way so that no uncertainty arises due to the measurement process. In spite these difficulties some authors have conducted experimental investigations on random dynamical systems. Kompella and Bernhard [22] measured 57 structure-borne frequency response functions at driver microphones for different pickup trucks. Fahy [23, page 275] reported measurements of FRFs on 41 nominally identical beer cans. Both of these experiments show variability in nominally identical engineered systems. Friswell et al. [24] reported two experiments where random systems were 'created' in the laboratory for the purpose of model validation. The first experiment used a randomly moving mass on a free-free beam and the second experiment comprised a copper pipe with uncertain internal pressure. Fifty nominally identical random samples were created and tested for both experiments.

This paper and its companion [1] describes two experimental studies that may be used to test methods of uncertainty quantification across the frequency range. The tests are closely controlled and the uncertainty can be considered to be 'known' for all practical purposes. This allows one to model uncertainty, propagate it through dynamical models and compare the results with this experimentally obtained data. The experiment described in this paper uses a fixed-fixed beam with 12 masses placed at random locations. The total *random mass* is about 2% of the total mass of the beam and this experiment simulates *random errors* in the mass matrix. One hundred nominally identical dynamical systems are created and individually tested in the Bristol Laboratory for Advanced Dynamic Engineering (BLADE). The model of the beam and experimental setup are described in section 2. The experimental method to test one hundred nominally identical structures are discussed in section 3. In section 4 the probabilistic characteristics of the amplitude and phase of the measured frequency response functions are discussed in the low, medium and high frequency ranges. In section 5 the experimental system with random mass distribution is numerically simulated using the Euler-Bernoulli beam theory and Monte Carlo simulation. In section 6 the mean and standard deviation of the amplitude and phase of the experimentally measured frequency response functions are compared with Monte Carlo simulation results. The key results and the contributions of this work are discussed section 7. The data presented here are available on the world wide web for research purposes. The web address is http://engweb.swan.ac.uk/~adhikaris/uq/. This data may be used to validate different uncertainty quantification and propagation methods in structural dynamics.

2 System Model and Experimental Setup

A steel beam with uniform rectangular cross-section is used for the experiment. The physical and geometrical properties of the steel beam are shown in Table 1. The beam is actually

Beam Properties	Numerical values
Length (L)	1200 mm
Width (b)	40.06 mm
Thickness (t_h)	2.05 mm
Mass density (ρ)	7800 kg/m^3
Young's modulus (E)	2.0×10^5 MPa
Cross sectional area ($a = bt_h$)	8.212×10^{-5} m^2
Moment of inertia ($I = 1/12bt_h^3$)	2.876×10^{-11} m^4
Mass per unit length (ρ_l)	0.641 kg/m
Bending rigidity (EI)	5.752 Nm^2
Total weight	0.7687 kg

Table 1
Material and geometric properties of the beam considered for the experiment

a 1.5m long ruler made of mild steel. The use of a ruler ensures that the masses may be easily placed at predetermined locations. The ruler is clamped between 0.05m and 1.25m so that the effective length of the vibrating beam is 1.2m. The overall experimental setup is shown in Figure 1. The end clamps are bolted to two heavy steel blocks, which in turn are fixed to a

Fig. 1. The test rig for the fixed-fixed beam.

rigid table with bolts as shown in Figure 2. The clamping arrangements are aimed at providing

fixed-fixed boundary conditions. The edges of both the solid metal blocks are sharpened to

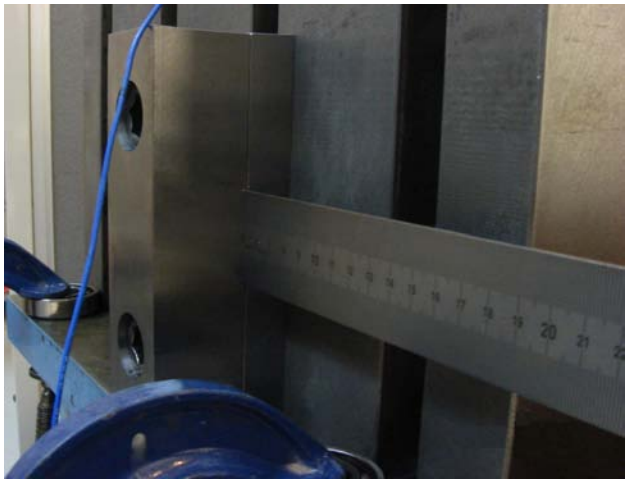

(a) Left end

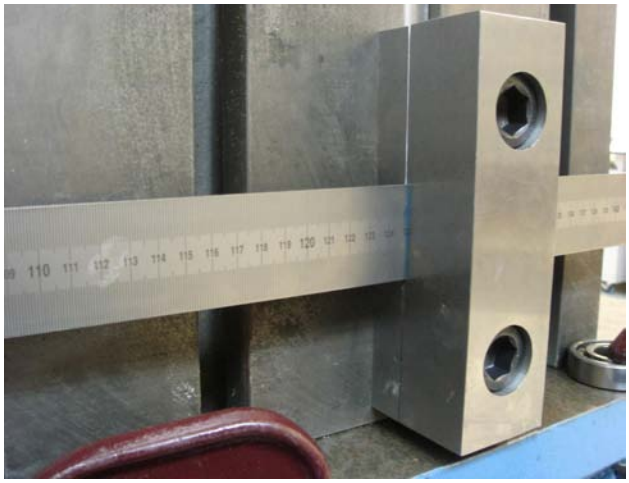

(b) Right end

Fig. 2. The clamping arrangements at the two ends of the beam. The clamping arrangement is aimed at providing fixed-fixed boundary conditions.

ensure that no rotation is allowed beyond the true 'end' of the beam. It is should be emphasized that it is, in general, extremely difficult to ensure there is no residual stress in a clamped or any other constrained system. Due to the fixed nature of the supports and flexibility of the beam, our initial tests show that the beam was in compression and was buckling in the first mode (the first natural frequency turned out to be close to zero and significantly lower than predicted by beam theory). The length between the supports was adjusted to minimize the compression or tension in the beam. Because the supports were not disturbed during the entire test spanning 100 realizations, we expect that the residual stress did not change from sample to sample.

Twelve equal masses are used to simulate a randomly varying mass distribution. The masses are actually magnets so that they can be easily attached at any location on the steel beam. These magnets are cylindrical in shape, with a length of 12.0mm and a diameter of 6.0mm. Some of the attached masses for a sample realization are shown in Figure 3. Each mass weights 2g so that the total variable mass is 1.6% of the mass of the beam. The location of the 12 masses are assumed to be between 0.2m and 1.0m from the left end of the beam. A uniform distribution with 100 samples is used to generate the mass locations. The mean and the standard deviations of the mass locations are given by

$$\bar{\mathbf{x}}_m = [0.2709, 0.3390, 0.3972, 0.4590, 0.5215, 0.5769, \\ 0.6398, 0.6979, 0.7544, 0.8140, 0.8757, 0.9387]\,\mathrm{m} \quad (2)$$

Fig. 3. The attached masses (magnets) at random locations. In total 12 masses, each weighting 2g, are used.

and

$$\sigma_{\mathbf{x}_m} = [0.0571, 0.0906, 0.1043, 0.1034, 0.1073, 0.1030, \\ 0.1029, 0.1021, 0.0917, 0.0837, 0.0699, 0.0530]\,\mathrm{m} \quad (3)$$

The variation of the locations of the 12 masses are shown in Figure 4.

3 Experimental Methodology

Experimental modal analysis [25–27] is used in this work. The three main components of the implemented experimental technique are (a) the excitation of the structure, (b) the sensing of the response, and (c) the data acquisition and processing. In this experiment a shaker was used (the make, model no. and serial no. are LDS V201, and 92358.3, respectively) to act as an impulse hammer. The usual manual impact hammer was not used because of the difficulty in ensuring the impact occurs at exactly at the same location with the same force for every sample run. The shaker generates impulses at a pulse interval of 20s and a pulse width of 0.01s. Using the shaker in this way eliminates, as far as possible, any uncertainties arising from the input forces. This innovative experimental technique is designed to ensure that the resulting uncertainty in the response arises purely due to the random locations of the attached masses. Figure 5 shows the arrangement of the shaker. A hard steel tip is used for the hammer to increase the frequency range of excitation. The beam material was relatively 'soft' compared to the hard steel tip, resulting in indentation marks. To avoid this problem a small circular brass plate weighting 2g is attached to the beam to take the impact from the shaker. The details of the force transducer attached to the shaker is given in Table 2.

In this experiment three accelerometers are used as the response sensors. The locations of the three sensors are selected such that two of them are near the two ends of the beam and

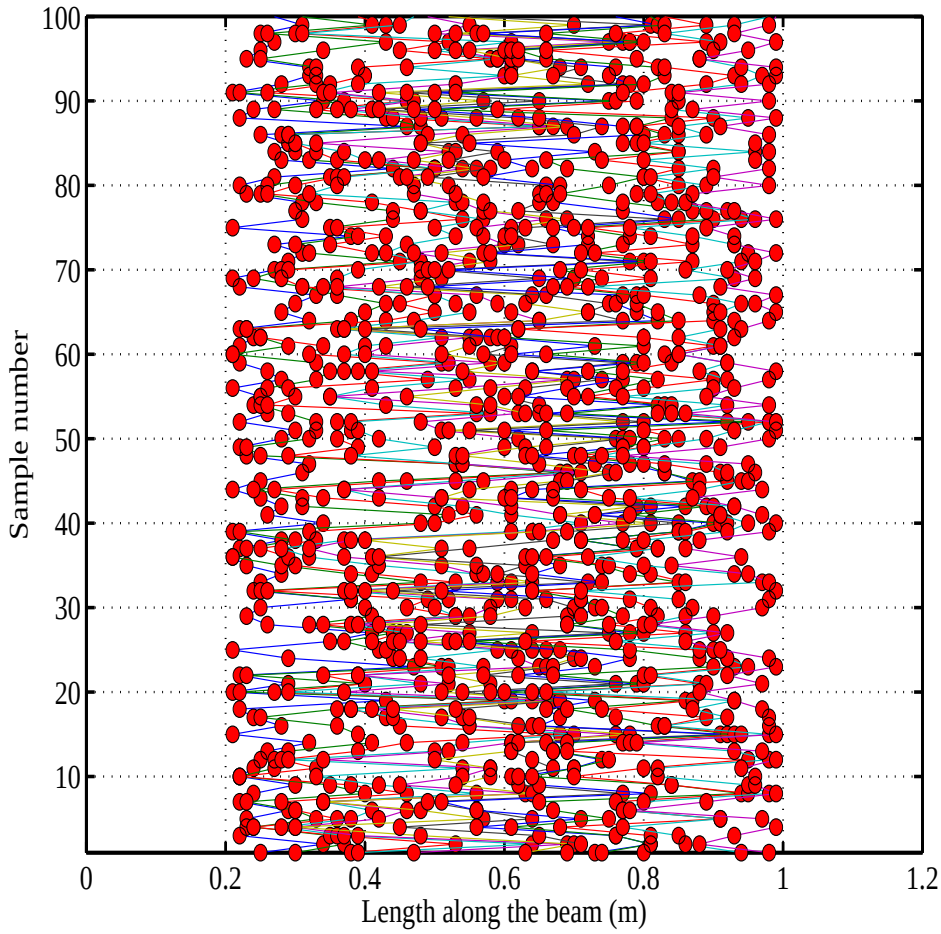

Fig. 4. All 100 samples of the locations of the 12 masses along the length of the beam. For each of the 100 samples, the 12 magnets are placed in these locations and the FRFs are measured.

one is at the exciter location, near the middle of the beam, so that driving-point frequency response function may be obtained. The exact locations are calculated such that the nodal lines of the first few bending modes are avoided. The details of the accelerometers, including their locations, are shown in Table 2. Small holes are drilled into the beam and the three

Role	Model & Serial number	Position from the left end	Channel	Sensitivity
Sensor (accelerometer)	PCB 333M07 SN 25948	23 cm (Point1)	1	98.8 mV/g
Sensor (accelerometer)	PCB 333M07 SN 26018	50 cm (Point2)	2	101.2 mV/g
Sensor (accelerometer)	PCB 333M07 SN 25942	102 cm (Point3)	3	97.6 mV/g
Actuator (force transducer)	PCB 208C03 21487	50 cm (Point2)	4	2.24 mV/N

Table 2
The details of the accelerometers and the force transducer for the beam experiment.

accelerometers are attached by bolts through these holes.

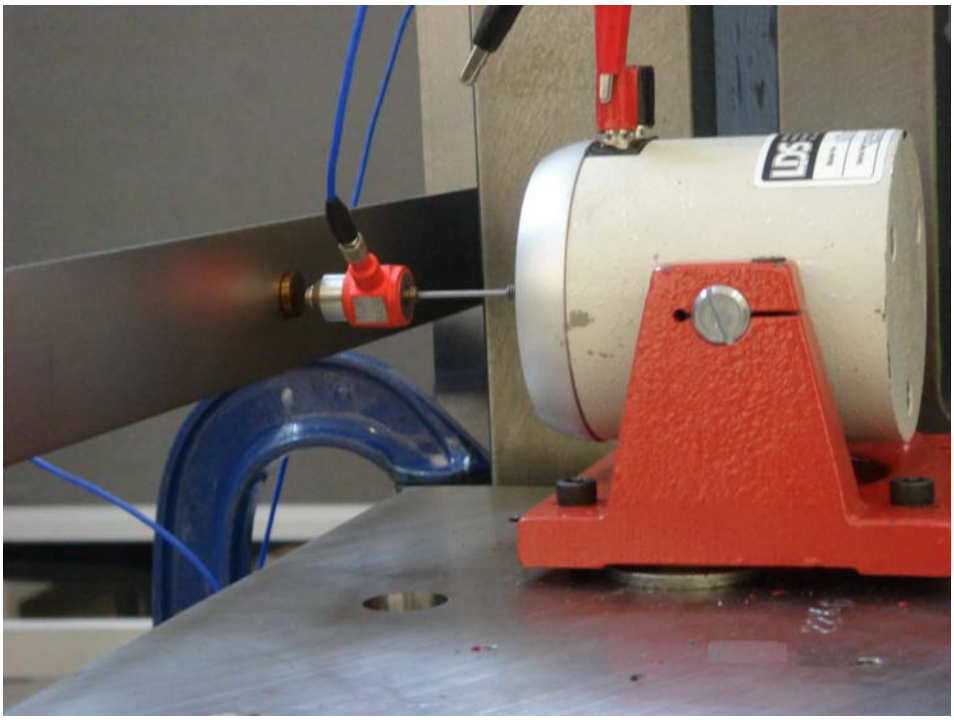

Fig. 5. The shaker is used as an impulse hammer which in turn is controlled via Simulink^{TM}and dSpace^{TM}. A hard steel tip was used and small brass plate weighting 2g is attached to the beam to take the impact from the shaker.

The signal from the force transducer is amplified using a KISTLER type 5134 amplifier (with settings Gain: 100, Filter: 10K and Bias: Off) while the signals from the accelerometers are directly input into a 32 channel LMS^{TM} system. For data acquisition and processing, LMS Test Lab 5.0 is used. In Impact Scope, the bandwidth is set to 8192 Hz with 8192 spectral lines (i.e., 1.00 Hz resolution). The steel tip used in the experiment only gives clean data up to approximately 4500 Hz, and thus 4500 Hz is used as the upper limit of the frequency in the measured frequency response functions. The data logged beyond 4500 Hz should be ignored.

4 Results and discussions

4.1 Amplitude spectra

In this paper we will discuss results corresponding to point 1 (a cross FRF) and point 2 (the driving-point FRF) only. Results for the other points are not shown to save space but can be obtained from the uploaded data file. Figure 6 shows the amplitude of the frequency response function (FRF) at point 1 (see Table 2 for the location) of the beam without any masses (the baseline model). In the same figure 100 samples of the amplitude of the FRF are shown together with the ensemble mean, 5% and 95% probability lines. Figures 6(b)-(d) show the low, medium and high-frequency response separately, obtained by zooming around the appropriate

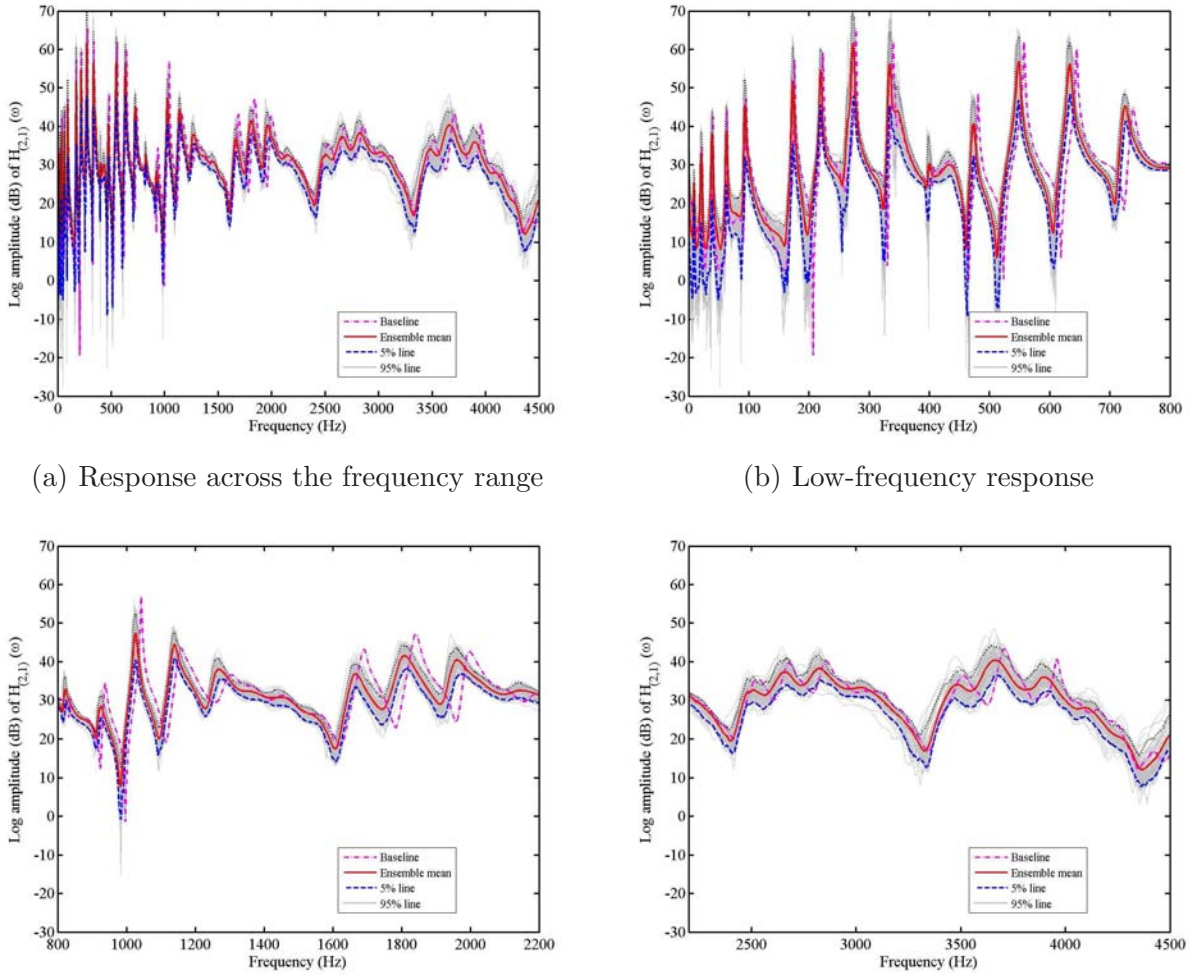

(a) Response across the frequency range

(b) Low-frequency response

(c) Medium-frequency response

(d) High-frequency response

Fig. 6. Experimentally measured amplitude of the FRF of the beam at point 1 (23 cm from the left end) with 12 randomly placed masses. 100 FRFs, together with the ensemble mean, 5% and 95% probability lines are shown.

frequency ranges in Figure 6(a). There are, of course, no fixed and definite boundaries between the low, medium and high-frequency ranges. Here we have selected $0 - 0.8$kHz as the low-frequency vibration, $0.8 - 2.2$kHz as the medium-frequency vibration and $2.2 - 4.5$kHz as the high-frequency vibration. These frequency boundaries are selected on the basis of the qualitative nature of the response and devised purely for the presentation of the results. The experimental approach discussed here is independent of these selections. The ensemble mean follows the result of the baseline system closely only in the low frequency range. In the higher modes, the mean natural frequencies are lower than the baseline system. This is because the mass of the baseline system is lower than the random system realizations. The relative variability of the amplitude of the FRF remains more or less constant in the mid and high frequency ranges. Equivalent results for point 2 (the driving-point FRF, see Table 2 for the

location) are shown in Figure 7. The general trend of the results is similar to that of point

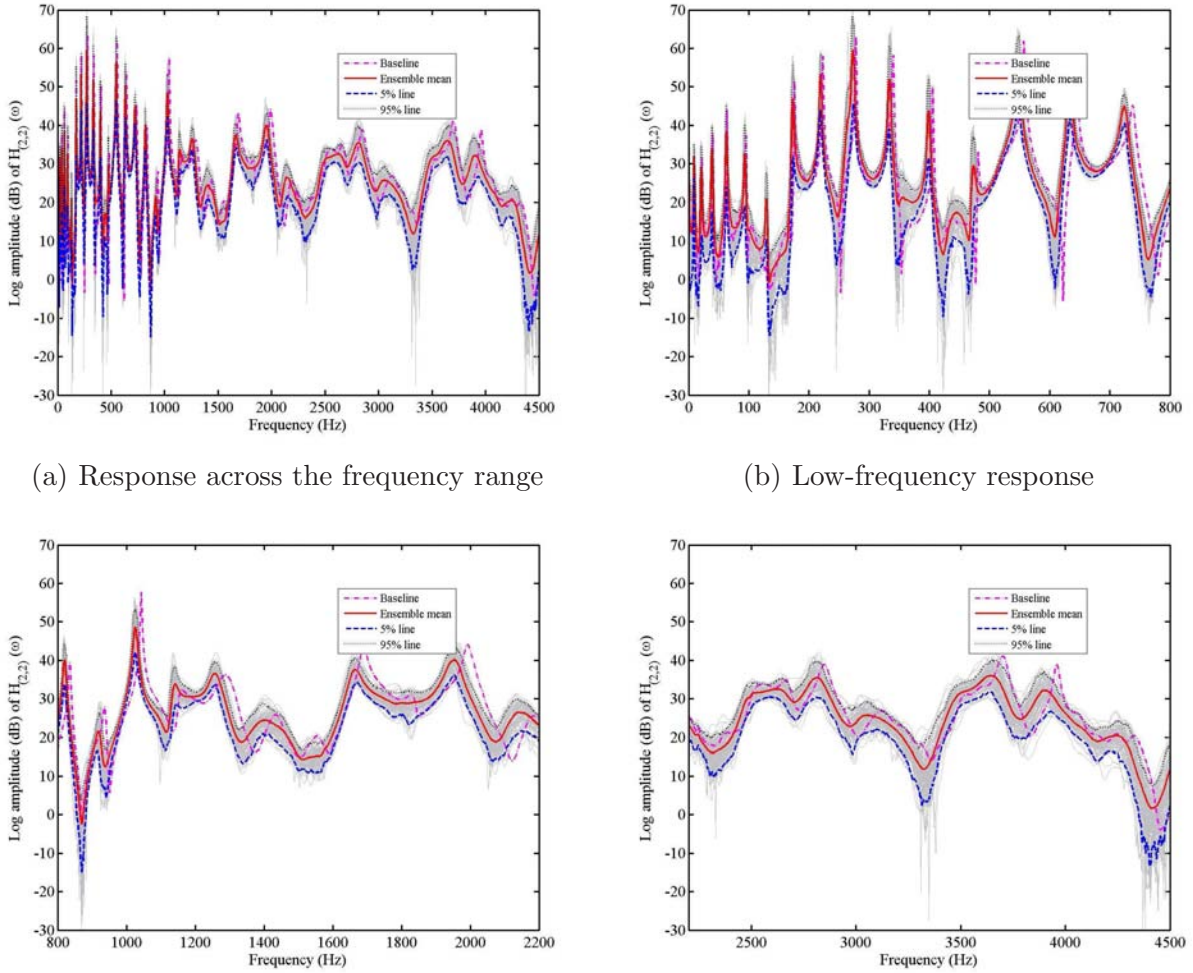

(a) Response across the frequency range

(b) Low-frequency response

(c) Medium-frequency response

(d) High-frequency response

Fig. 7. Experimentally measured amplitude of the FRF of the beam at point 2 (the driving-point FRF, 50 cm from the left end) with 12 randomly placed masses. 100 FRFs, together with the ensemble mean, 5% and 95% probability lines are shown.

1. The measured FRF data up to 4.5 KHz as shown here is significantly noise-free, since the hard steel tip used was able to excite the whole frequency range. The experimental data shown throughout the paper is the 'raw data' (that is, without any filtering) obtained directly from the LMS system.

4.2 Phase spectra

Figure 9 shows the phase of the frequency response function (FRF) at point 1 (see Table 2 for the location) of the beam without any masses (the baseline model). In the same figure 100 samples of the phase of the FRF are shown together with the ensemble mean, 5% and

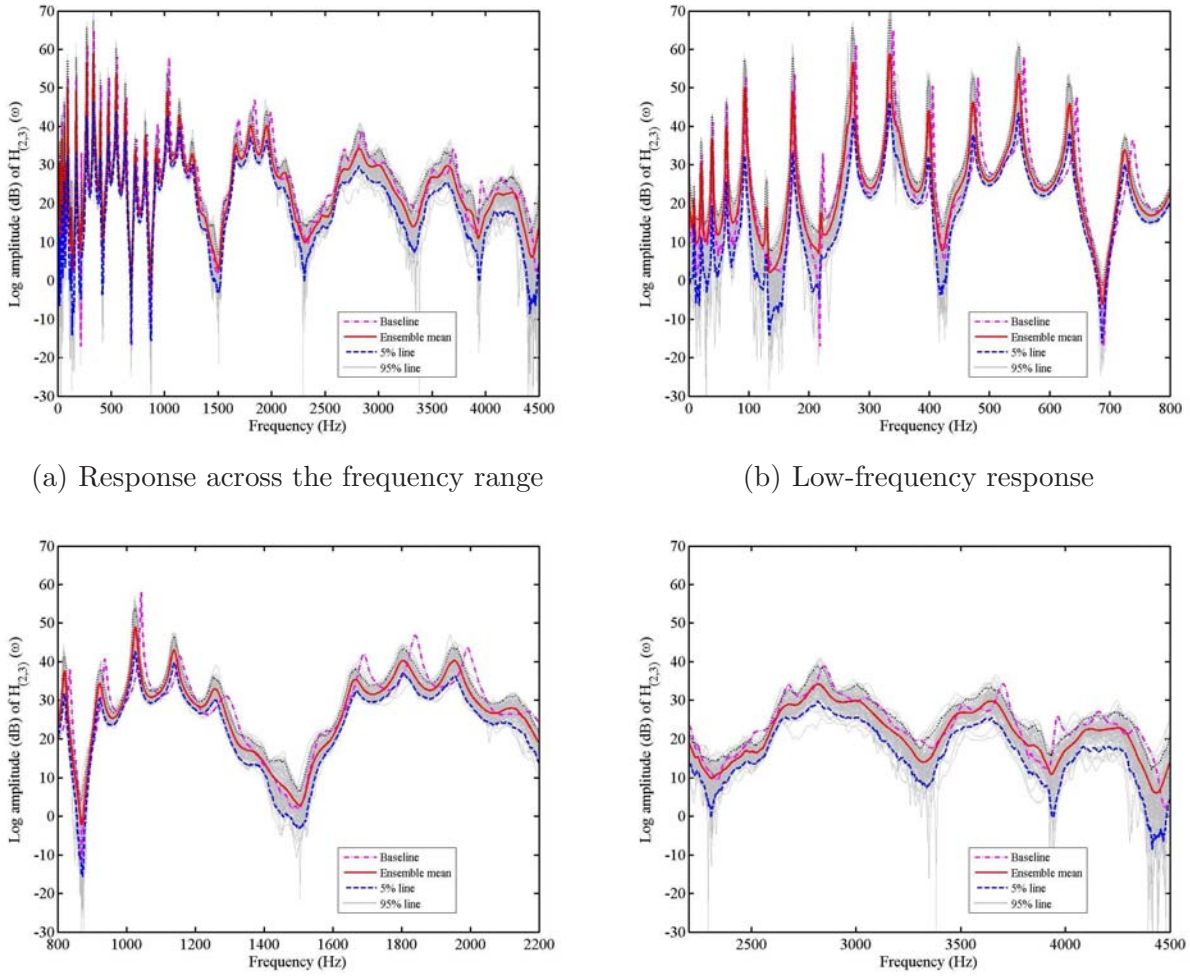

(a) Response across the frequency range

(b) Low-frequency response

(c) Medium-frequency response

(d) High-frequency response

Fig. 8. Experimentally measured amplitude of the FRF of the beam at point 3 with 12 randomly placed masses (102 cm from the left end). 100 FRFs, together with the ensemble mean, 5% and 95% probability lines are shown.

95% probability lines. Figures 9(b)-(d) show the phase in low, medium and high-frequency separately, obtained by zooming around the appropriate frequency ranges in Figure 9(a). The ensemble mean follows the result of the baseline system closely only in the low frequency range. In the higher modes, one can observe a clear phase-lag. This is again due to the fact that the baseline system has lower mass compared to the mass of the random system realizations.

The relative variability of the phase of the FRF remains more or less constant in the mid and high frequency ranges. Equivalent results for point 2 (the driving-point FRF, see Table 2 for the location) are shown in Figure 10. Because this is the phase of driving-point FRF, its general characteristics is different from the cross FRF shown in Figure 9. The variability is also observed to be slightly higher compared to the phase of the cross-FRF.

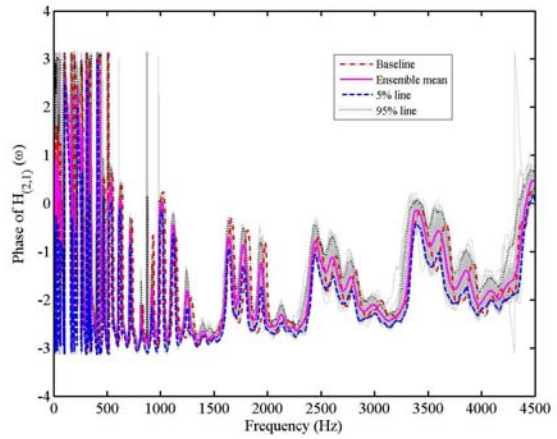

(a) Phase across the frequency range

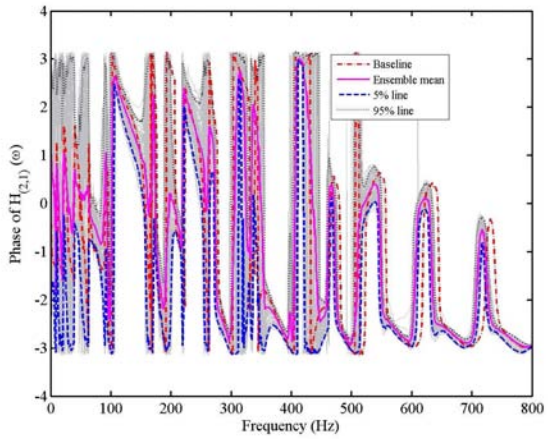

(b) Low-frequency response

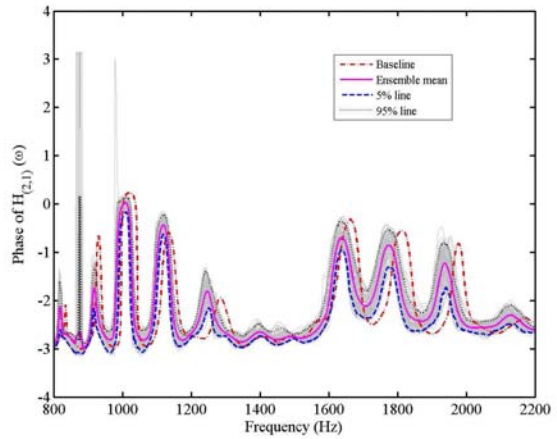

(c) Medium-frequency response

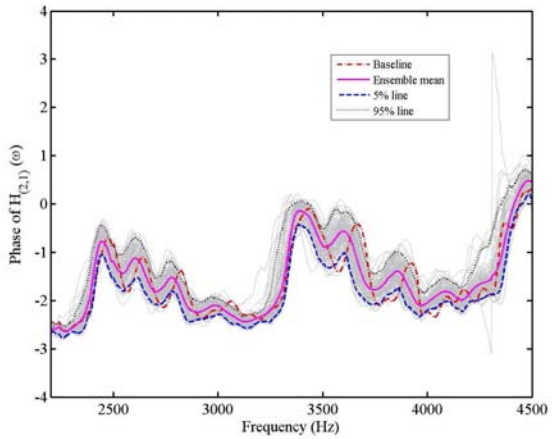

(d) High-frequency response

Fig. 9. Experimentally measured phase of the FRF of the beam at point 1 (23 cm from the left end) with 12 randomly placed masses. 100 FRFs, together with the ensemble mean, 5% and 95% probability lines are shown.

5 Numerical simulation

In this section we model the beam and the attached masses at random locations using Monte Carlo simulation. As shown in Figure 1, the beam is uniform and clamped at both ends. We include the 12 randomly located masses, the mass of the three accelerometers (6g each) and the mass of the small circular brass plate (2g) to take the impact from the impulse hammer. The equation of motion of the mass loaded beam can be expressed as

$$EI\frac{\partial^4 w(x,t)}{\partial x^4} + m\,\ddot{w}(x,t) + \sum_{j=1}^{12} m_r\,\ddot{w}(x_{r_j},t) + \sum_{j=1}^{3} m_a\,\ddot{w}(x_{a_j},t) + m_b\,\ddot{w}(x_b,t) = f(x,t). \quad (4)$$

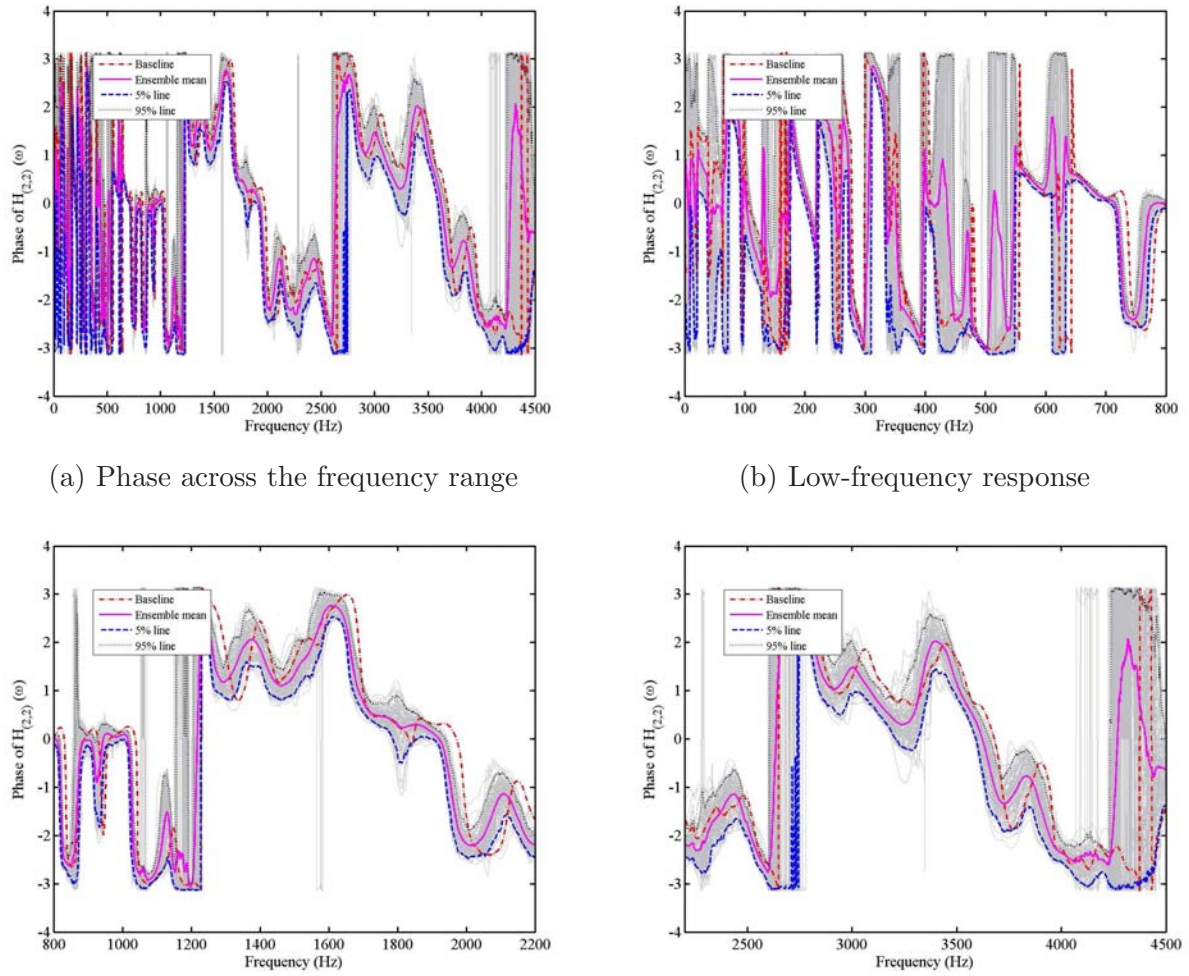

(a) Phase across the frequency range

(b) Low-frequency response

(c) Medium-frequency response

(d) High-frequency response

Fig. 10. Experimentally measured phase of the FRF of the beam at point 2 (the driving-point FRF, 50 cm from the left end) with 12 randomly placed masses. 100 FRFs, together with the ensemble mean, 5% and 95% probability lines are shown.

where EI is the bending stiffness of the beam, x is the spatial coordinate along the length of the beam, t is the time, $w(x,t)$ is the time depended transverse deflection of the beam, $f(x,t)$ is the applied time depended load on the beam, m is the mass per unit length of the beam and L is the length of the beam. An in-house finite element code was developed to implement the discretized version of equation (4).

In the numerical calculations 120 elements are used and the resulting finite element model has 238 degrees-of-freedom. Half of the modes, that is 119 modes, are used in the calculation of the frequency response functions. One intuitive way to quantify uncertainty in linear dynamical systems is to use the statistical overlap factor [28], defined as the ratio of the standard deviation of the natural frequencies to the average spacing of the natural frequencies. Figure 12 shows the mean, standard deviation and statistical overlap factors of the natural frequencies of the

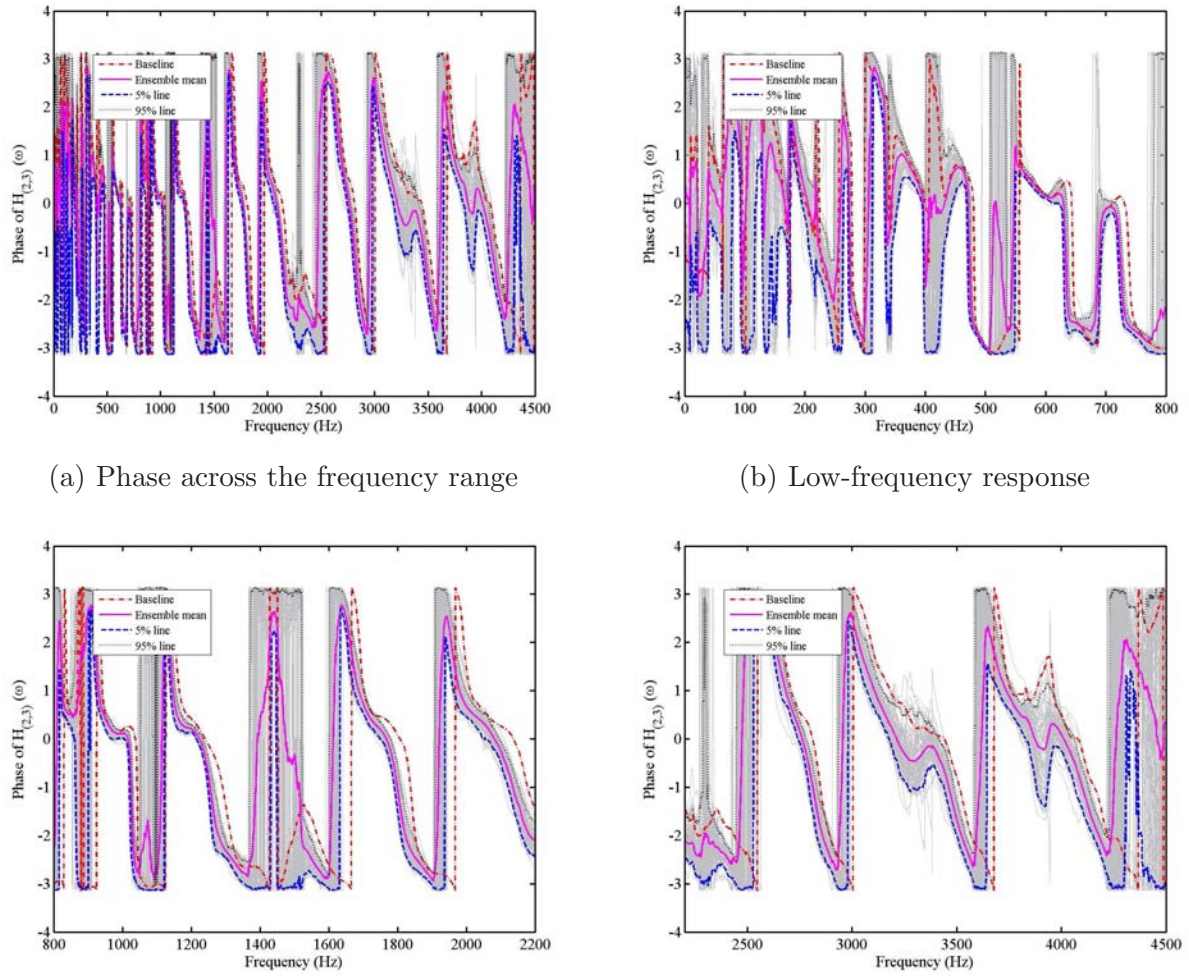

(a) Phase across the frequency range

(b) Low-frequency response

(c) Medium-frequency response

(d) High-frequency response

Fig. 11. Experimentally measured phase of the FRF of the beam at point 3 with 12 randomly placed masses (102 cm from the left end). 100 FRFs, together with the ensemble mean, 5% and 95% probability lines are shown.

beam obtained using Monte Carlo simulation. From Figure 12(a) observe that the standard deviation of the natural frequencies are quite small compared to the mean values. This is also reflected in Figure 12(b) where it can be observed that, on average, the statistical overlap factors of the system is below 0.5. This implies that we do not expect significant mid-frequency or high-frequency type of behaviour. Experimental results shown in Figures 6 and 7 support this conclusion.

5.1 Amplitude spectra

For the frequency response function calculation, a modal damping factor of 1.5% is assumed for all of the modes. The location of 100 sets of mass positions used for the experiment are

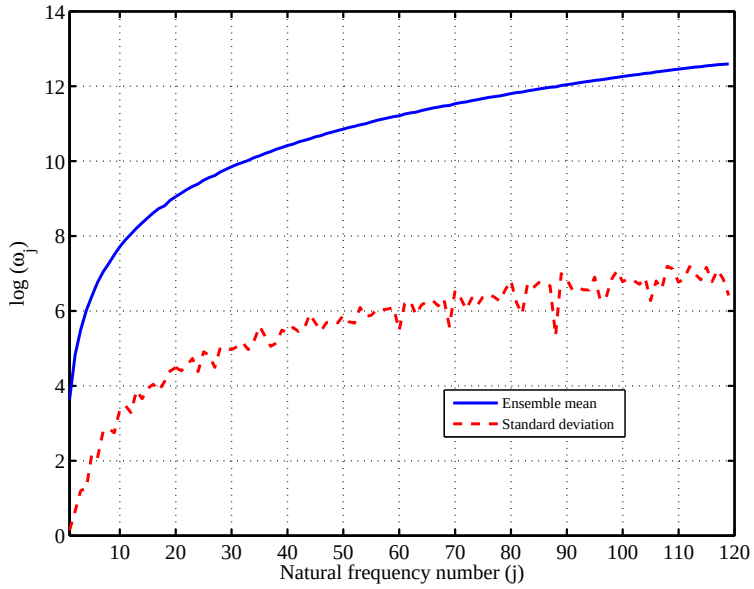

(a) Natural frequency statistics

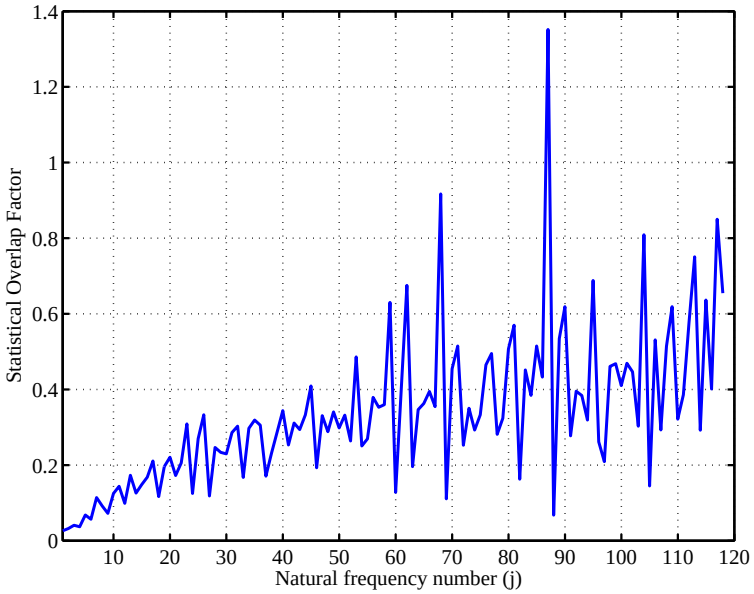

(b) Statistical overlap factors

Fig. 12. Mean, standard deviation and statistical overlap factor of the natural frequencies of the beam with random mass.

again used for the Monte Carlo simulation. Figure 13 shows the amplitude of the frequency response function (FRF) at point 1 (see Table 2 for the location) of the beam without any masses (the baseline model). In the same figure 100 samples of the amplitude of the FRF are shown together with the ensemble mean, 5% and 95% probability lines. Figures 13(b)-(d) show the low, medium and high-frequency response separately, obtained by zooming around the appropriate frequency ranges in Figure 13(a). Equivalent results for point 2 (the driving-point FRF, see Table 2 for the location) are shown in Figure 14. For both the points, the

ensemble mean follows the result of the baseline system fairly closely over the entire frequency range. This is somewhat different what observed in the experimental results. The relative variance of the amplitude of the FRF remains more or less constant in the mid and high frequency ranges, which is qualitatively similar to the experimental results.

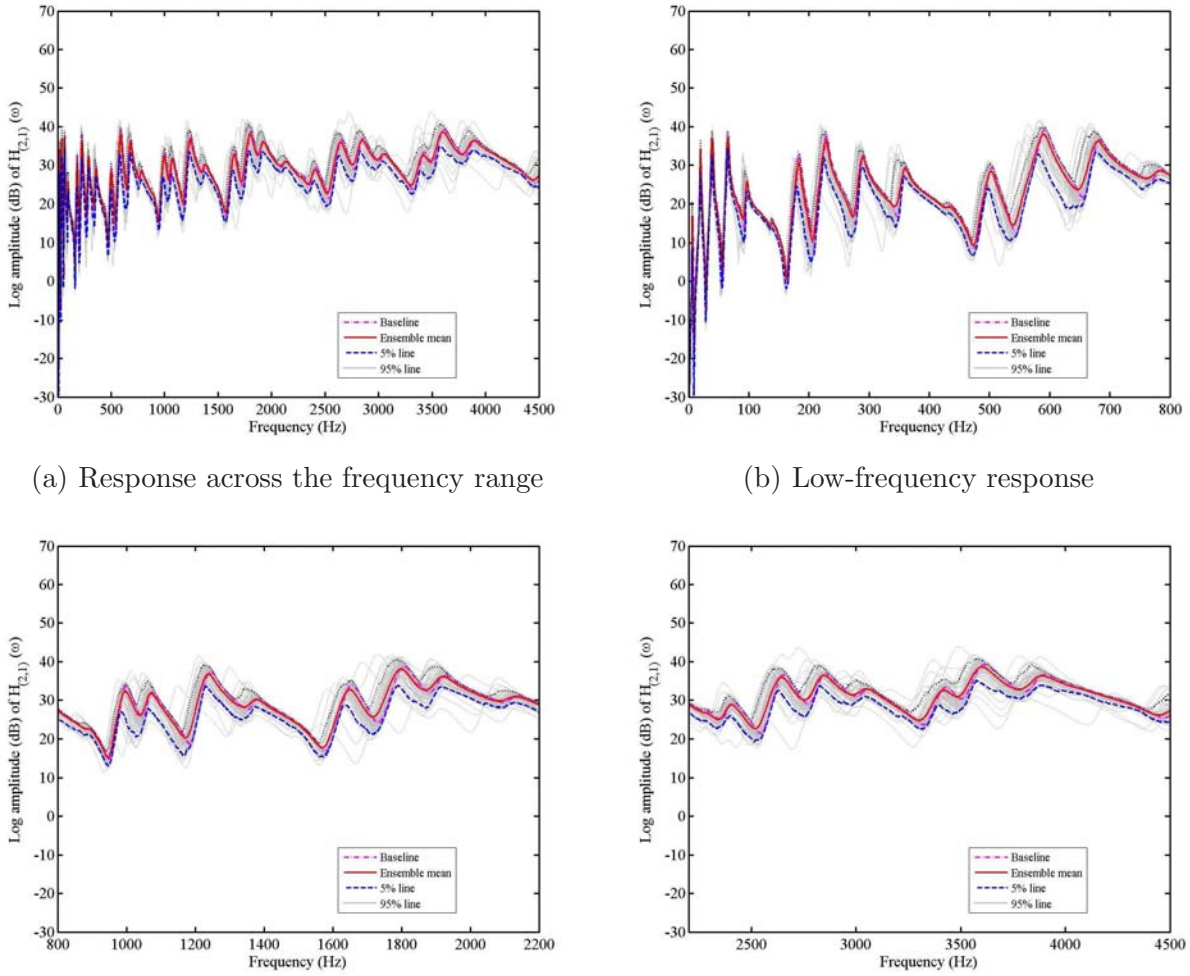

(a) Response across the frequency range

(b) Low-frequency response

(c) Medium-frequency response

(d) High-frequency response

Fig. 13. Numerically calculated amplitude of the FRF of the beam at point 1 (23 cm from the left end) with 12 randomly placed masses. 100 FRFs, together with the ensemble mean, 5% and 95% probability lines are shown.

5.2 Phase spectra

Figure 16 shows the phase of the frequency response function (FRF) at point 1 (see Table 2 for the location) of the beam without any masses (the baseline model). In the same figure 100 samples of the phase of the FRF are shown together with the ensemble mean, 5% and 95% probability lines. Figures 16(b)-(d) show the phase in low, medium and high-frequency

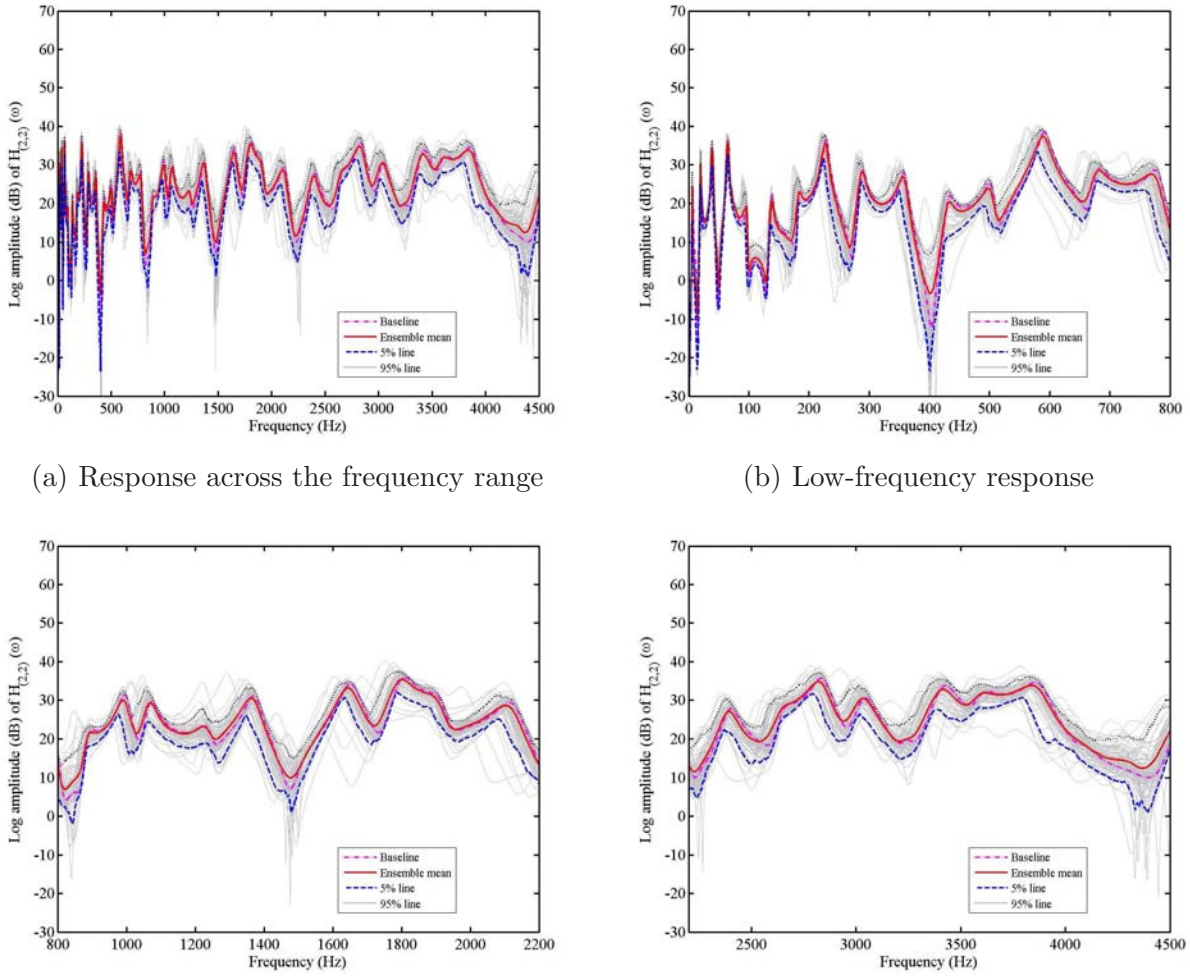

(a) Response across the frequency range

(b) Low-frequency response

(c) Medium-frequency response

(d) High-frequency response

Fig. 14. Numerically calculated amplitude of the FRF of the beam at point 2 (the driving-point FRF, 50 cm from the left end) with 12 randomly placed masses. 100 FRFs, together with the ensemble mean, 5% and 95% probability lines are shown.

separately, obtained by zooming around the appropriate frequency ranges in Figure 16(a). The ensemble mean follows the result of the baseline system closely except in few areas. The relative variability of the amplitude of the FRF remains more or less constant in the mid and high frequency ranges. Equivalent results for point 2 (the driving-point FRF, see Table 2 for the location) are shown in Figure 10. Because this is the phase of the driving-point FRF, its general characteristics are different from the cross FRF shown in Figure 9. The variability is also observed to be slightly higher compared to the phase of the cross-FRF. Overall, the numerical results show a similar trend to the experiential results.

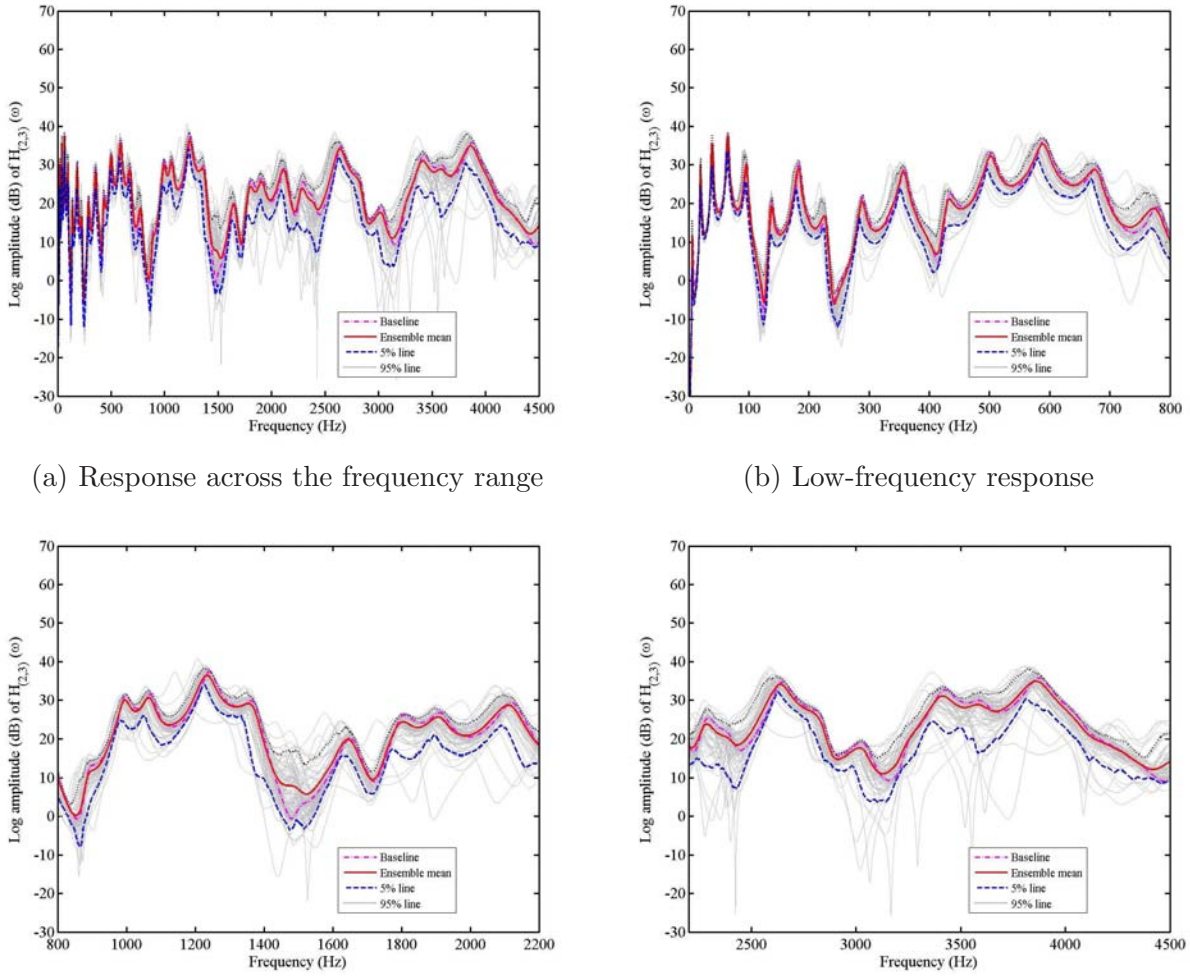

(a) Response across the frequency range

(b) Low-frequency response

(c) Medium-frequency response

(d) High-frequency response

Fig. 15. Numerically calculated amplitude of the FRF of the beam at point 3 with 12 randomly placed masses (102 cm from the left end). 100 FRFs, together with the ensemble mean, 5% and 95% probability lines are shown.

6 Comparisons between numerical and experimental results

6.1 Amplitude spectra

It is useful to compare the experimental results with the Monte Carlo simulation results. Figure 19 compares the ensemble mean and standard deviation of the amplitude of the frequency response function (FRF) at point 1 obtained from the experiment and Monte Carlo simulation. Figures 19(b)-(d) show the low, medium and high-frequency response separately, obtained by zooming around the appropriate frequency ranges in Figure 19(a). To the best of the authors knowledge, this is perhaps the first time where direct comparison between experimental and analytical (simulation) results for stochastic dynamical systems have been

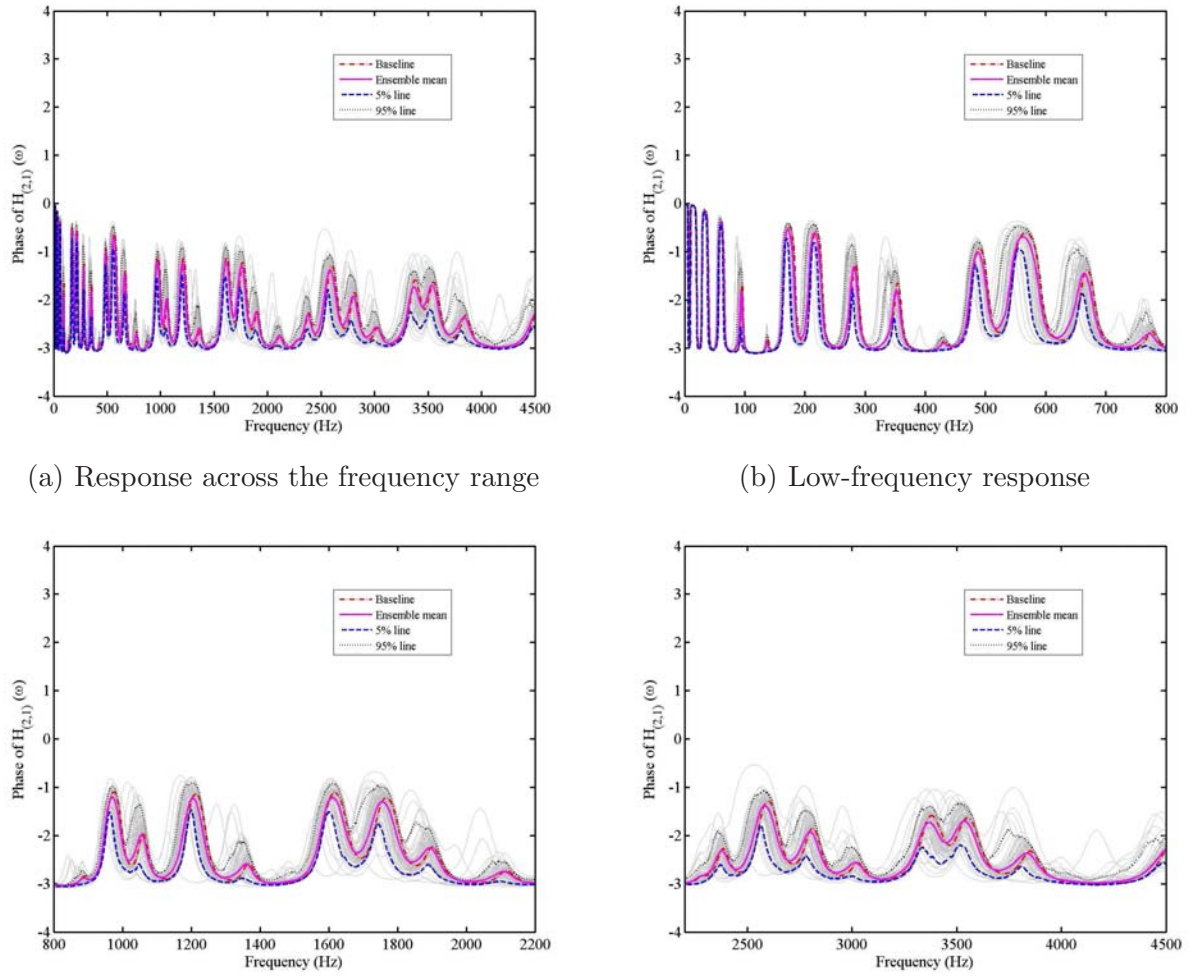

(a) Response across the frequency range

(b) Low-frequency response

(c) Medium-frequency response

(d) High-frequency response

Fig. 16. Numerically calculated phase of the FRF of the beam at point 1 (23 cm from the left end) with 12 randomly placed masses. 100 FRFs, together with the ensemble mean, 5% and 95% probability lines are shown.

reported. The standard deviation of the amplitude of the FRF reaches a peak at the system natural frequencies, which is also predicted by the numerical simulation. Qualitatively the simulation results agree well with the experimental results. The main reason for the discrepancies, especially in the low frequency regions, is probably due to the incorrect value of the damping factors. In the simulation study a constant damping factor of 1.5% is assumed for all of the modes. Ideally one should measure modal damping factors from experimental measurements for all of the samples and for as many modes as possible and perhaps take an average across the samples for every mode. Equivalent comparisons for point 2 (the driving-point FRF) are shown in Figure 20. For both points, the experimental mean and standard deviation in the low frequency range is quite high compared to numerical results. This can again be attributed to the wrong values of modal damping factors in the analytical model since the pattern of

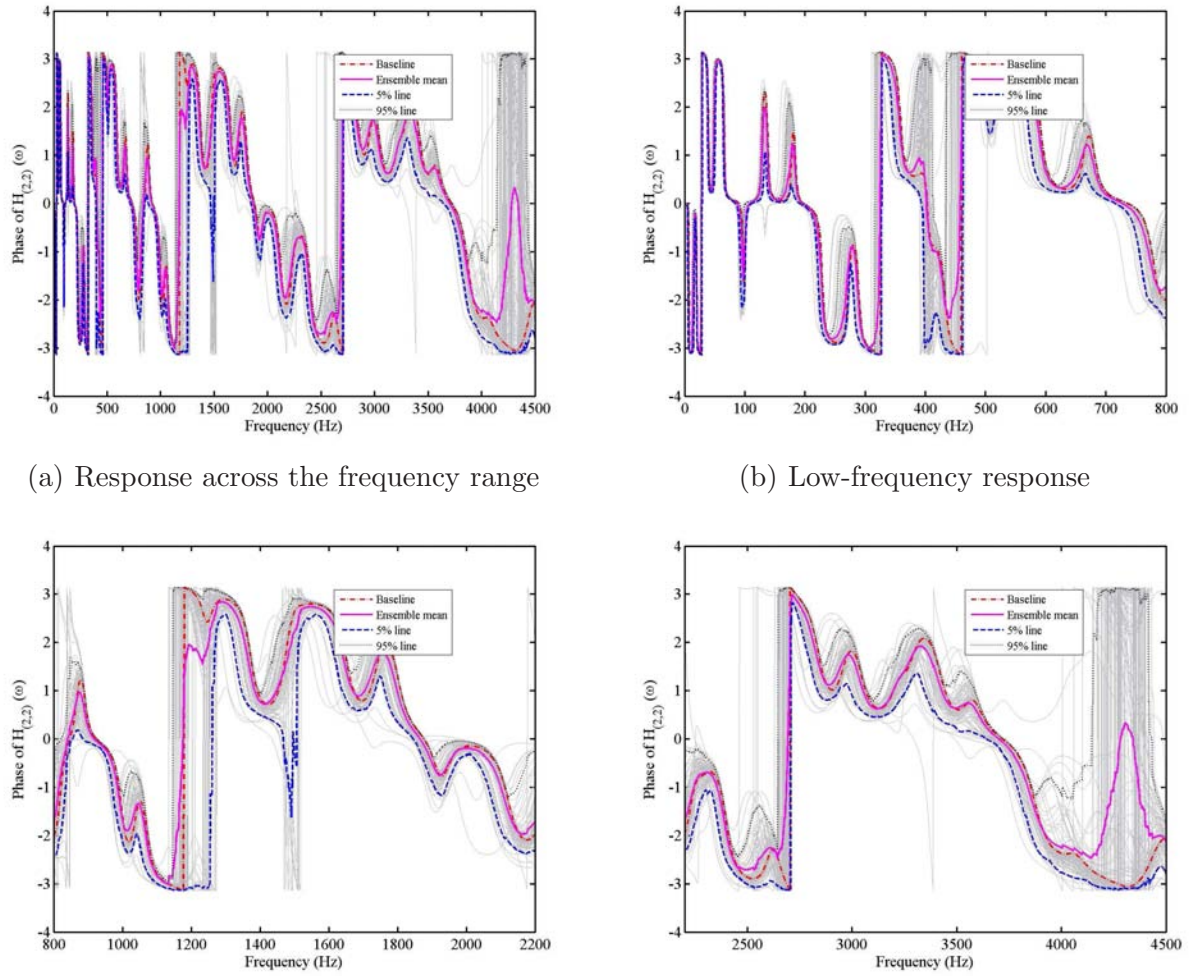

(a) Response across the frequency range

(b) Low-frequency response

(c) Medium-frequency response

(d) High-frequency response

Fig. 17. Numerically calculated phase of the FRF of the beam at point 2 (the driving-point FRF, 50 cm from the left end) with 12 randomly placed masses. 100 FRFs, together with the ensemble mean, 5% and 95% probability lines are shown.

the peaks are strikingly similar but they are separated in 'height'. This is a clear indication that the damping values are incorrect in the simulation model. Therefore, one of the key outcomes of this experimental study is that wrong values of the modal damping factors can lead to significant errors in the response variance prediction even if everything else is performed correctly.

6.2 Phase spectra

Figure 22 compares the ensemble mean and standard deviation of the phase of the frequency response function at point 1 obtained from the experiment and Monte Carlo simulation. Figures 22(b)-(d) show the low, medium and high-frequency response separately, obtained by

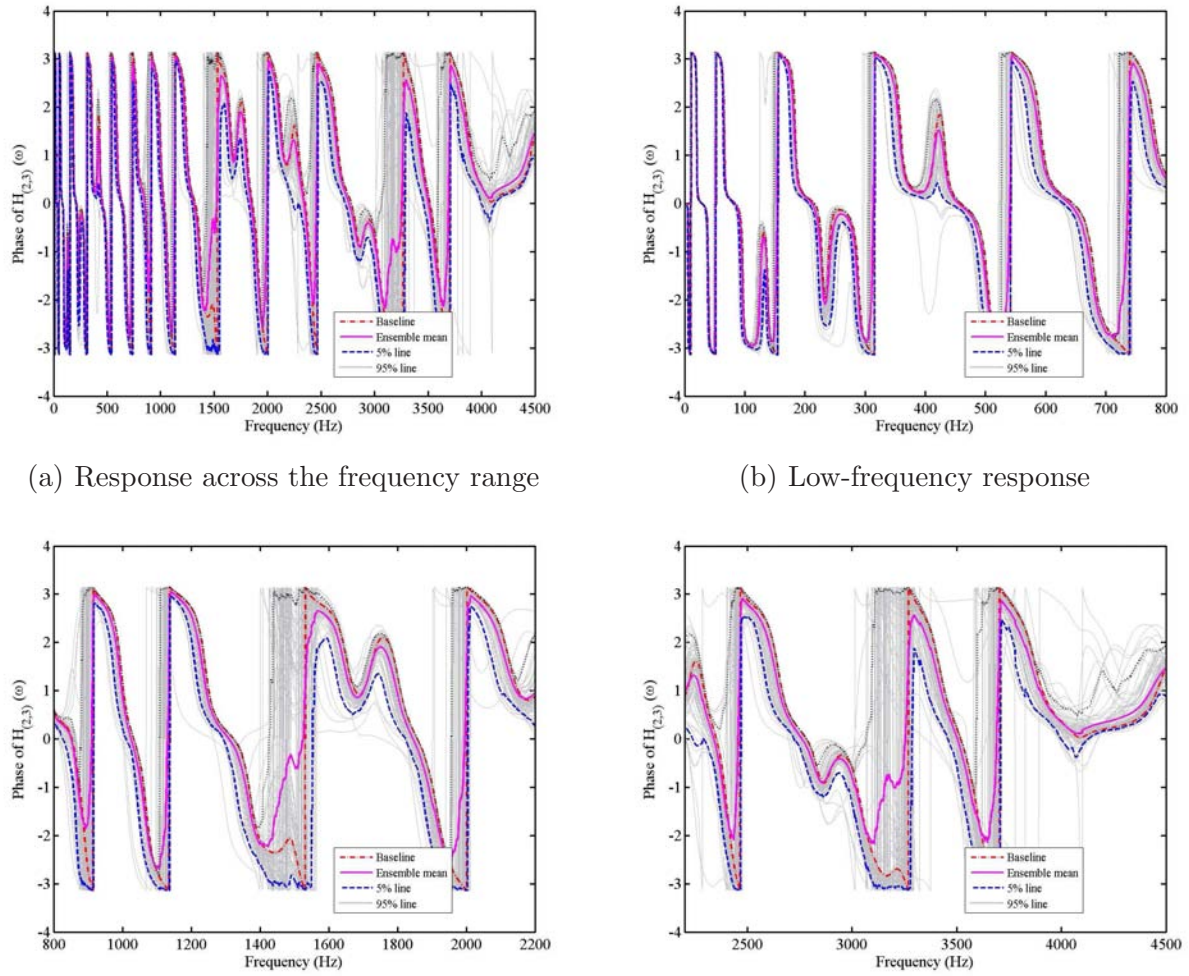

(a) Response across the frequency range

(b) Low-frequency response

(c) Medium-frequency response

(d) High-frequency response

Fig. 18. Numerically calculated phase of the FRF of the beam at point 3 with 12 randomly placed masses (102 cm from the left end). 100 FRFs, together with the ensemble mean, 5% and 95% probability lines are shown.

zooming around the appropriate frequency ranges in Figure 22(a). Except in the low frequency range, the standard deviation of the phase of the FRF is very small and the experimental and simulation results agree well. The patterns of the mean results from the experiment and simulation is very similar. The discrepancy is again primarily due to the incorrect damping model in the numerical results. Equivalent comparisons for point 2 (the driving-point FRF) are shown in Figure 23. Observe that the agreement of the simulated results with the experimental results is better than for the cross-FRF shown before. One can clearly see similar trends in both the mean and the standard deviation. Taken overall, qualitatively the simulation results agree well with the experimental results.

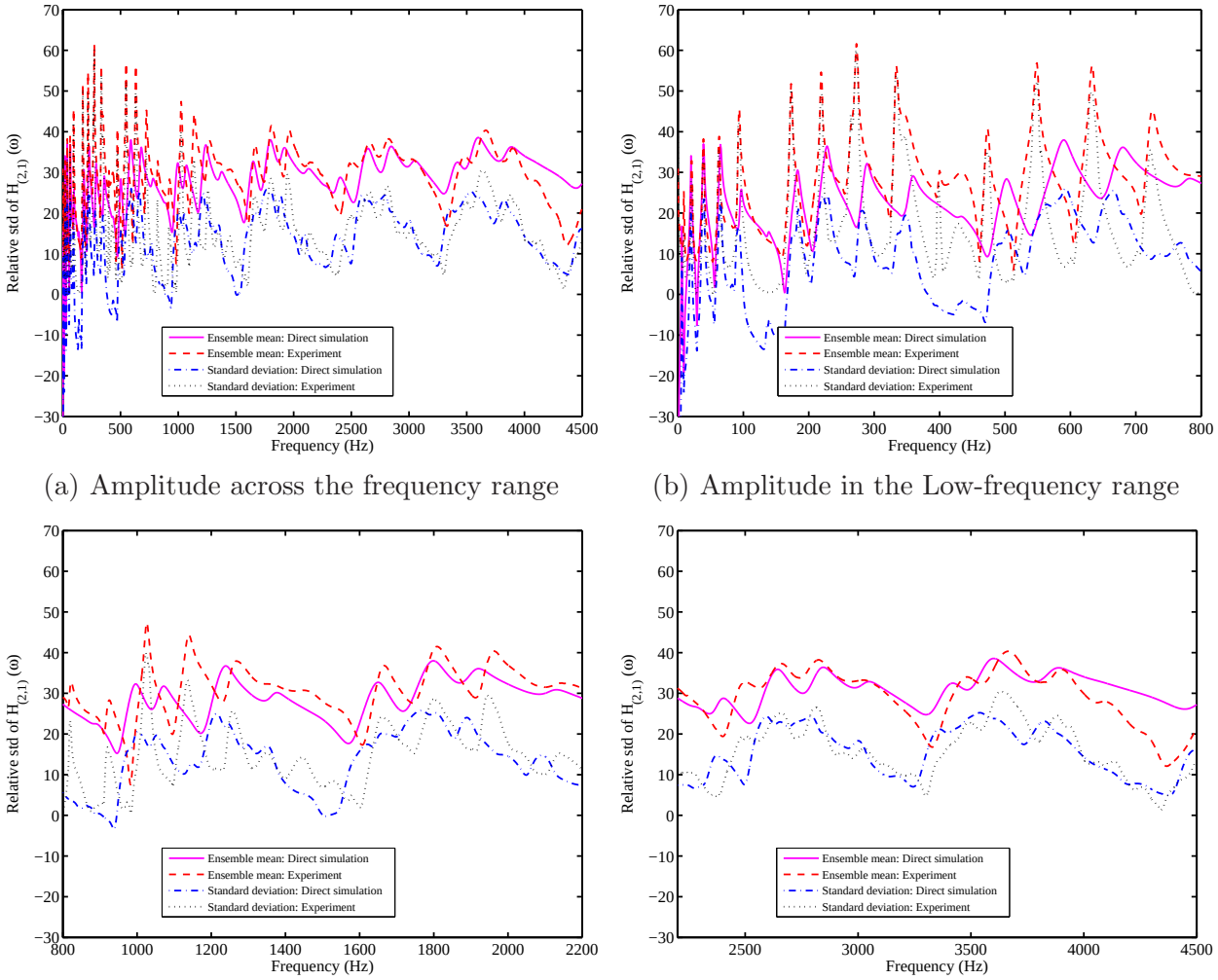

(a) Amplitude across the frequency range

(b) Amplitude in the Low-frequency range

(c) Amplitude in the Medium-frequency range

(d) Amplitude in the High-frequency range

Fig. 19. Comparison of the mean and standard deviation of the amplitude of the beam at point 1 (23 cm from the left end) using direct Monte Carlo simulation and experiment.

7 Conclusions

This paper has described an experiment that may be used to study methods to quantify uncertainty in the dynamics of structures. The fixed-fixed beam is very easy to model and the results of a one hundred sample experiment with randomly placed masses are described in this paper. One hundred nominally identical beams are created and individually tested using experimental modal analysis. Special measures have been taken so that the uncertainty in the response only arises from the randomness in the mass locations and the experiments are repeatable with minimum changes. Such measures include, but are not limited to (a) the use of a shaker as an impact hammer to ensure a consistent force and location for all of the tests, (b) the use of a ruler to minimize the error in measuring the mass locations, (c) the use of magnets as attached masses and (d) the use of a hard steel tip and a small brass plate

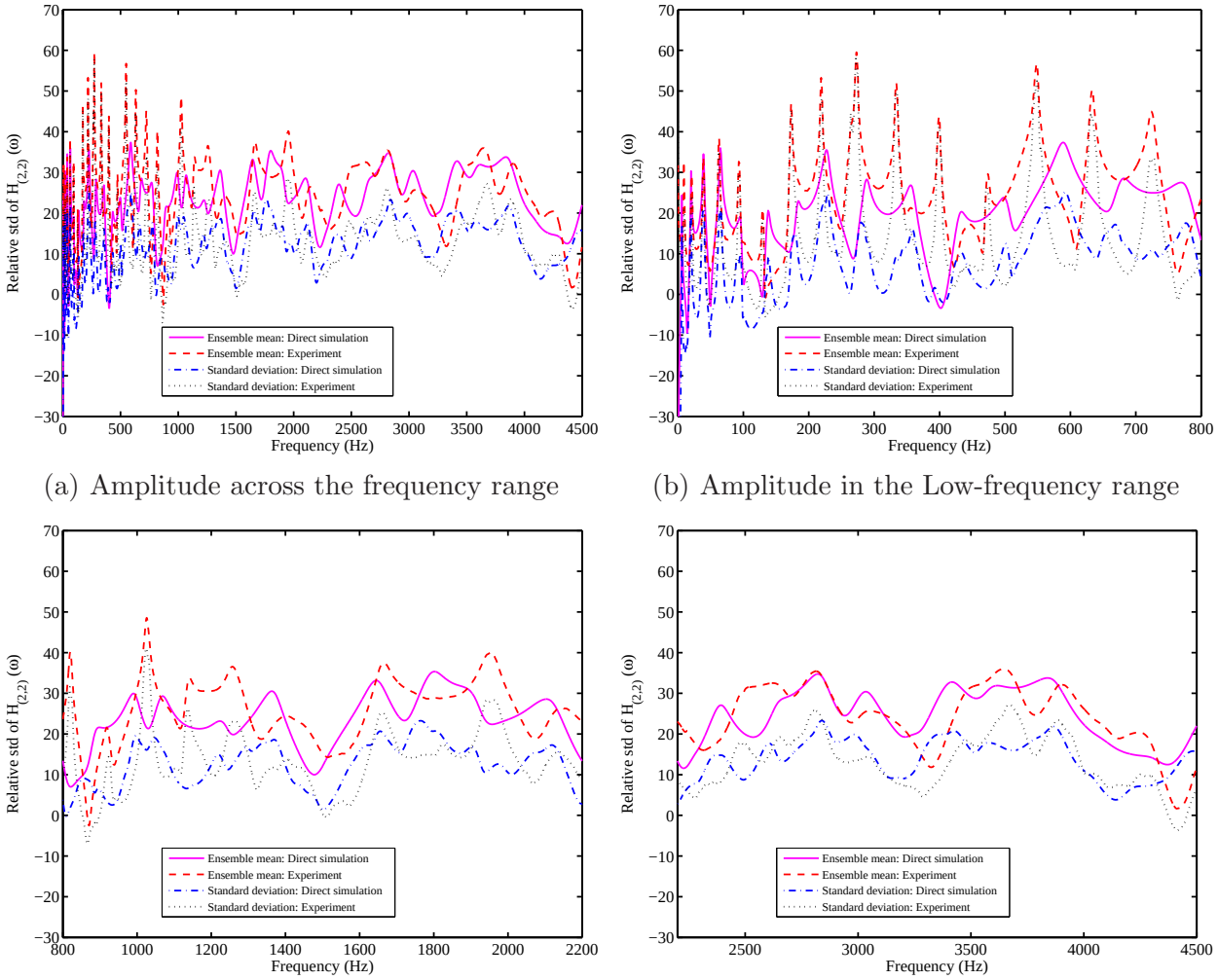

(a) Amplitude across the frequency range

(b) Amplitude in the Low-frequency range

(c) Amplitude in the Medium-frequency range

(d) Amplitude in the High-frequency range

Fig. 20. Comparison of the mean and standard deviation of the amplitude of the beam at point 2 (the driving-point FRF, 50 cm from the left end) using direct Monte Carlo simulation and experiment.

on the flexible beam to obtain relatively noise-free data up to 4.5KHz. The statistics of the frequency response functions measured at the three points are obtained for low, medium and high frequency ranges. More variability in the FRF at the high frequency range compared to the low frequency range is observed. This data may be used for the model validation and uncertainty quantification of dynamical systems. Of course one hundred set of samples is not enough for a reliable statistical analysis. But to the best of the authors knowledge, to date this is perhaps the most comprehensive set of experimentally measured response data available for stochastic dynamical systems.

The experimental results are directly compared with numerical Monte Carlo simulation. This is perhaps the first time where such a direct comparison between experimental and analytical (simulation) results for stochastic dynamical systems have been reported in stochastic mechanics literature. A finite element model of a simple Euler-Bernoulli beam is used in the

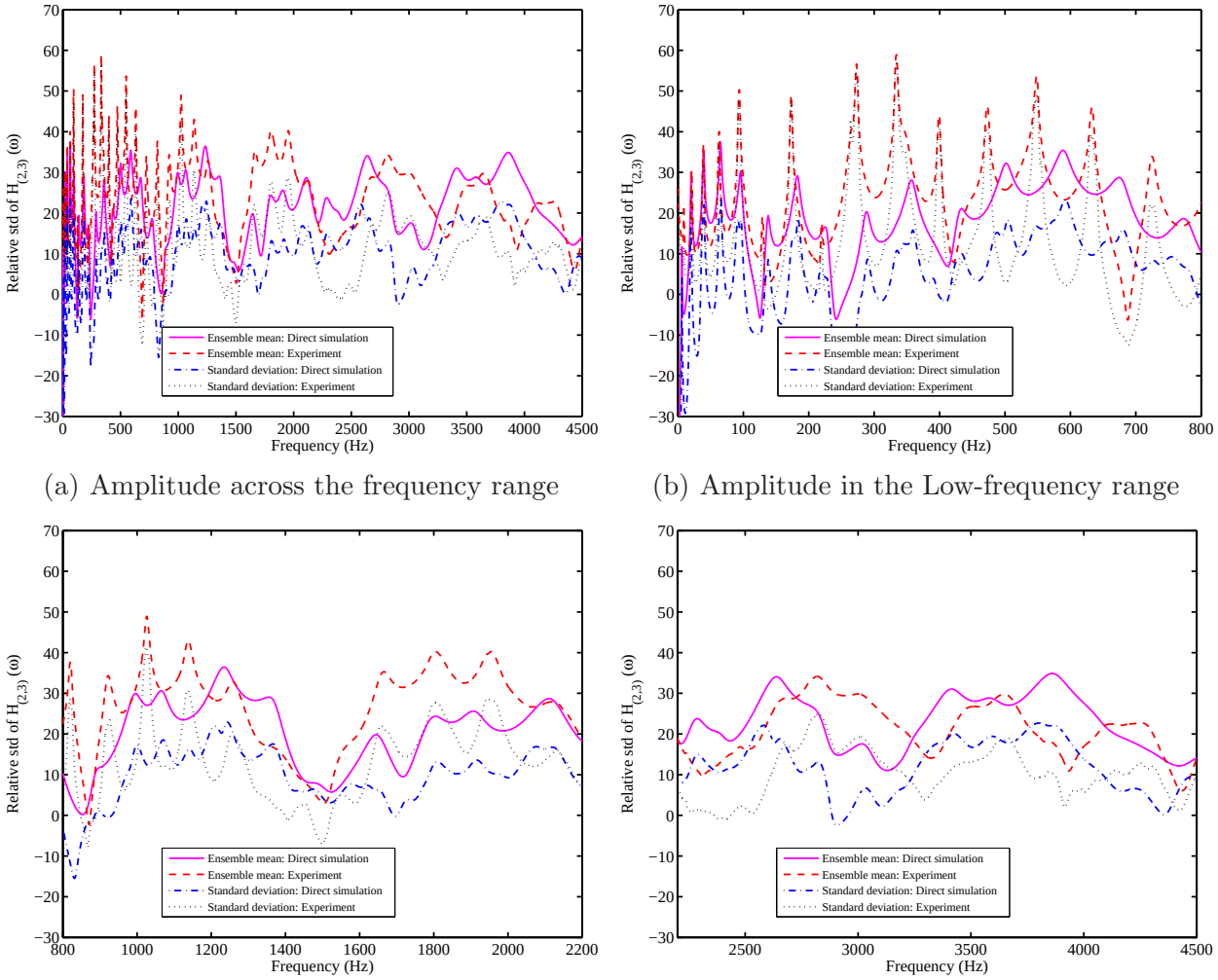

(a) Amplitude across the frequency range

(b) Amplitude in the Low-frequency range

(c) Amplitude in the Medium-frequency range

(d) Amplitude in the High-frequency range

Fig. 21. Comparison of the mean and standard deviation of the amplitude of the beam at point 3 (102 cm from the left end) using direct Monte Carlo simulation and experiment.

analytical work, and the pattern of the response mean and standard deviation obtained in the experimental analysis is predicted. The discrepancies between the two approaches are attributed to incorrect values for damping used in the numerical model. This suggests that correct damping values are crucial for the prediction of the response variance of stochastic dynamical systems.

Acknowledgements

SA gratefully acknowledges the support of the Engineering and Physical Sciences Research Council through the award of an Advanced Research Fellowship. MIF gratefully acknowledges the support of the Royal Society through a Royal Society-Wolfson Research Merit Award.

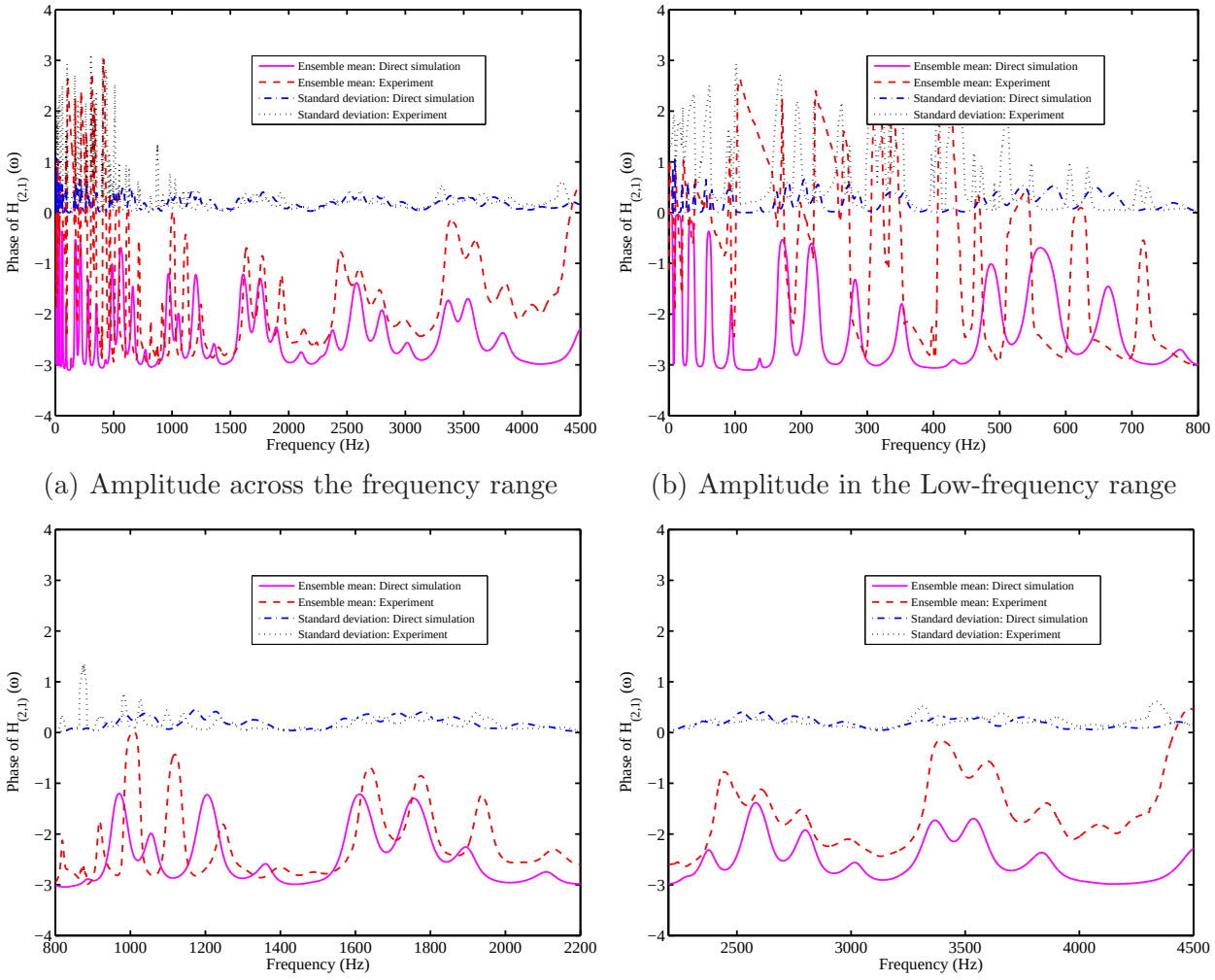

(a) Amplitude across the frequency range

(b) Amplitude in the Low-frequency range

(c) Amplitude in the Medium-frequency range

(d) Amplitude in the High-frequency range

Fig. 22. Comparison of the mean and standard deviation of the phase of the beam at point 1 (23 cm from the left end) using direct Monte Carlo simulation and experiment.

References

[1] Adhikari S, Friswell MI, Lonkar K, Sarkar A. Experimental case studies for uncertainty quantification in structural dynamics: Part 2, plate experiment. Probabilistic Engineering Mechanics 2007;Under review.

[2] Shinozuka M, Yamazaki F. Stochastic finite element analysis: an introduction. In *Stochastic structural dynamics: Progress in theory and applications*, Ariaratnam ST, Schueller GI, Elishakoff I, editors. London: Elsevier Applied Science 1998; .

[3] Ghanem R, Spanos P. *Stochastic Finite Elements: A Spectral Approach*. New York, USA: Springer-Verlag 1991.

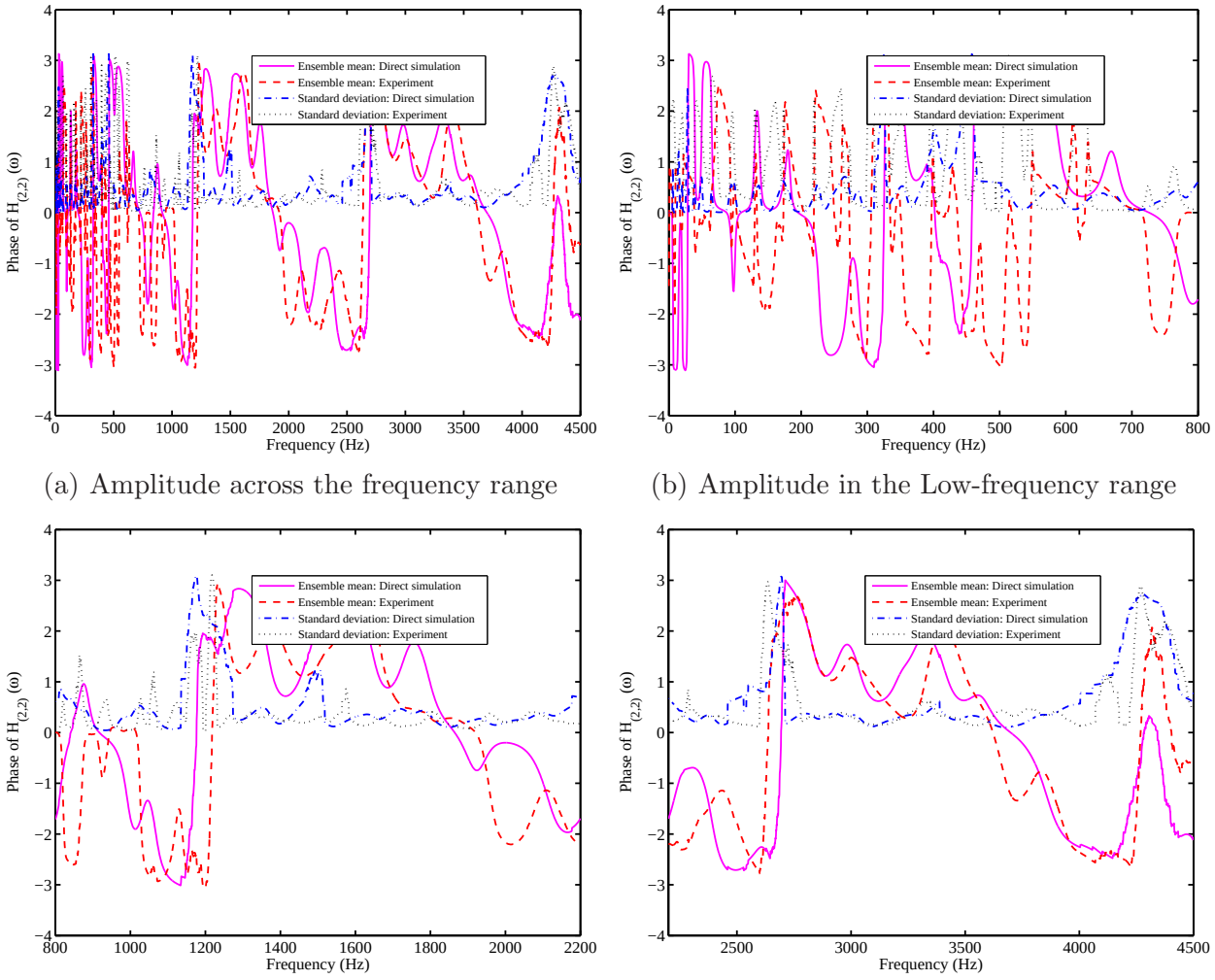

(a) Amplitude across the frequency range

(b) Amplitude in the Low-frequency range

(c) Amplitude in the Medium-frequency range

(d) Amplitude in the High-frequency range

Fig. 23. Comparison of the mean and standard deviation of the phase of the beam at point 2 (the driving-point FRF, 50 cm from the left end) using direct Monte Carlo simulation and experiment.

[4] Kleiber M, Hien TD. *The Stochastic Finite Element Method*. Chichester: John Wiley 1992.

[5] Manohar CS, Adhikari S. Dynamic stiffness of randomly parametered beams. Probabilistic Engineering Mechanics 1998;13(1):39–51.

[6] Adhikari S, Manohar CS. Dynamic analysis of framed structures with statistical uncertainties. International Journal for Numerical Methods in Engineering 1999;44(8):1157–1178.

[7] Adhikari S, Manohar CS. Transient dynamics of stochastically parametered beams. ASCE Journal of Engineering Mechanics 2000;126(11):1131–1140.

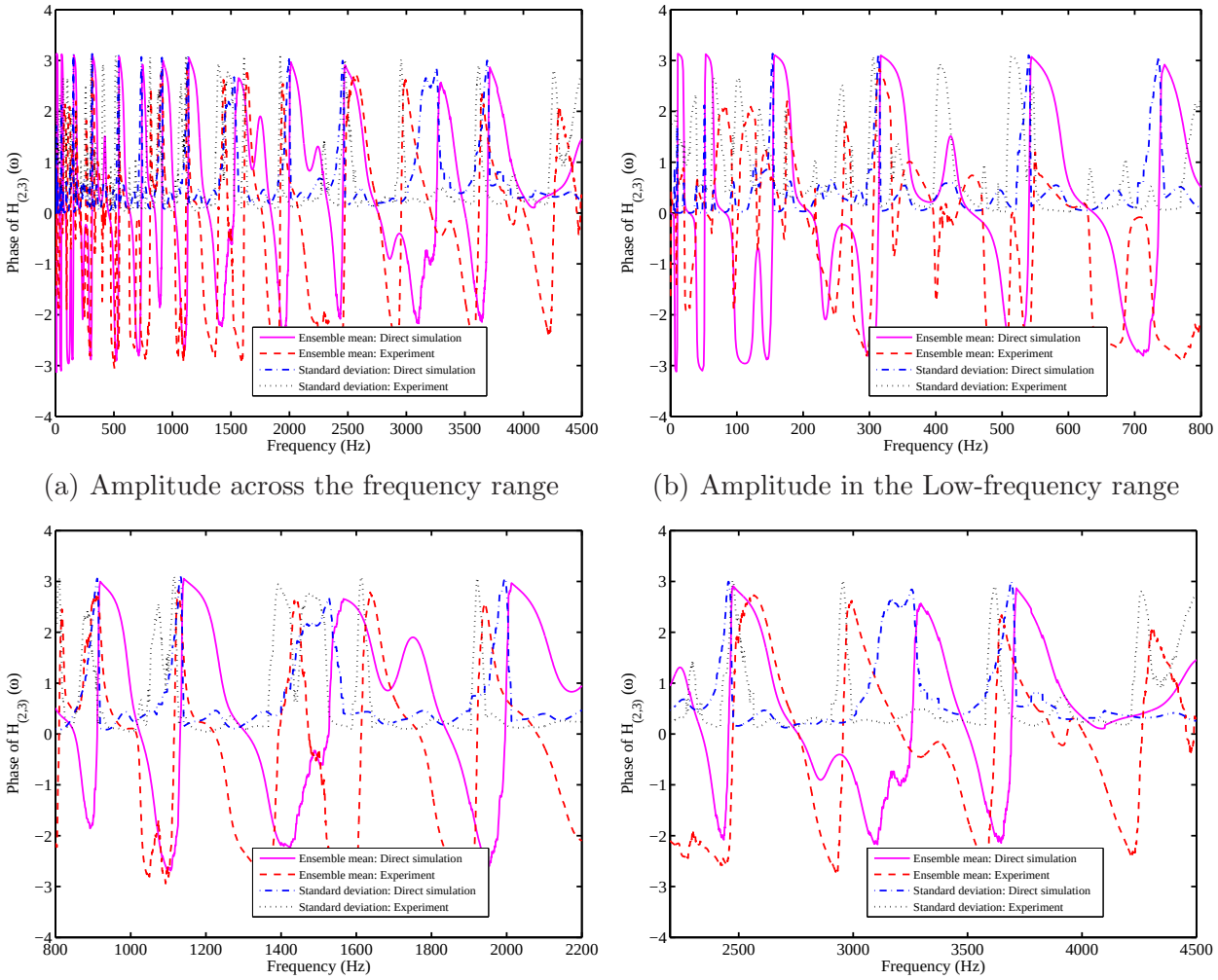

(a) Amplitude across the frequency range

(b) Amplitude in the Low-frequency range

(c) Amplitude in the Medium-frequency range

(d) Amplitude in the High-frequency range

Fig. 24. Comparison of the mean and standard deviation of the phase of the beam at point 3 (102 cm from the left end) using direct Monte Carlo simulation and experiment.

[8] Haldar A, Mahadevan S. *Reliability Assessment Using Stochastic Finite Element Analysis*. New York, USA: John Wiley and Sons 2000.

[9] Sudret B, Der-Kiureghian A. Stochastic Finite Element Methods and Reliability. Tech. Rep. UCB/SEMM-2000/08, Department of Civil & Environmental Engineering, University Of California, Berkeley 2000.

[10] Elishakoff I, Ren YJ. *Large Variation Finite Element Method for Stochastic Problems*. Oxford, U.K.: Oxford University Press 2003.

[11] Soize C. Non-Gaussian positive-definite matrix-valued random fields for elliptic stochastic partial differential operators. Computer Methods in Applied Mechanics and Engineering 2006;195(1-3):26–64.

[12] Adhikari S. A non-parametric approach for uncertainty quantification in elastodynamics. In *47th AIAA/ASME/ASCE/AHS/ASC Structures, Structural Dynamics & Materials Conference*. Newport, Rhode Island, USA 2006; .

[13] Adhikari S. Matrix variate distributions for probabilistic structural mechanics. AIAA Journal 2007;Accepted for publication.

[14] Matthies HG, Brenner CE, Bucher CG, Soares CG. Uncertainties in probabilistic numerical analysis of structures and solids - Stochastic finite elements. Structural Safety 1997; 19(3):283–336.

[15] Lyon RH, Dejong RG. *Theory and Application of Statistical Energy Analysis*. Boston: Butterworth-Heinmann, second edn. 1995.

[16] Keane AJ, Price WG. *Statistical Energy Analysis: An Overview With Applications in Structural Dynamics*. Cambridge, UK: Cambridge University Press 1997. First published in Philosophical Transactions of the Royal Society of London, series A, vol 346, pp. 429-554, 1994.

[17] Langley RS. A general derivation of the statistical energy analysis equations for coupled dynamic-systems. Journal of Sound and Vibration 1989;135(3):499–508.

[18] Langley RS, Bremner P. A hybrid method for the vibration analysis of complex structural-acoustic systems. Journal of the Acoustical Society of America 1999;105(3):1657–1671.

[19] Sarkar A, Ghanem R. Mid-frequency structural dynamics with parameter uncertainty. Computer Methods in Applied Mechanics and Engineering 2002;191(47-48):5499–5513.

[20] Sarkar A, Ghanem R. A substructure approach for the midfrequency vibration of stochastic systems. Journal of the Acoustical Society of America 2003;113(4):1922–1934. Part 1.

[21] Sarkar A, Ghanem R. Reduced models for the medium-frequency dynamics of stochastic systems. Journal of the Acoustical Society of America 2003;113(2):834–846.

[22] Kompella MS, Bernhard BJ. Measurement of the statistical variations of structural-acoustics characteristics of automotive vehicles. In *SAE Noise and Vibration Conference*. Warrendale, USA: Society of Automotive Engineers 1993; .

[23] Fahy F. *Foundations of Engineering Acoustics*. London, UK: Academic Press Inc., 2000.

[24] Friswell MI, Coote JA, Terrell MJ, Adhikari S, Fonseca JR, Lieven NAJ. Experimental Data for Uncertainty Quantification. In *Proceedings of the 23rd International Modal Analysis Conference (IMAC - XXIII)*. Orlando, Florida, USA: Society of Experimental Mechanics (SEM) 2005; .

[25] Ewins DJ. *Modal Testing: Theory and Practice*. Baldock, England: Research Studies Press, second edn. 2000.

[26] Maia NMM, Silva JMM, editors. *Theoretical and Experimental Modal Analysis*. Engineering Dynamics Series. Taunton, England: Research Studies Press 1997. Series Editor, J. B. Robetrs.

[27] Silva JMME, Maia NMM, editors. *Modal Analysis and Testing: Proceedings of the NATO Advanced Study Institute*, NATO Science Series: E: Applied Science. Sesimbra, Portugal 1998.

[28] Manohar CS, Keane AJ. Statistics of energy flow in one dimentional subsystems. Philosophical Transactions of Royal Society of London 1994;A346:525–542.

Nomenclature

$\mathbf{f}(t)$	forcing vector
$\mathbf{M}$, $\mathbf{C}$ and $\mathbf{K}$	mass, damping and stiffness matrices respectively
$\mathbf{q}(t)$	response vector
EI	bending stiffness of the beam
$f(x,t)$	applied time depended load on the beam
L	length of the beam
m	mass per unit length of the beam, $m = \rho A$
m_a	mass of an accelerometer, $m_a = 6$g
m_b	mass of the circular brass plate, $m_b = 2$g
m_r	added mass at random locations on the beam, $m_a = 2$g
n	number of degrees of freedom
t	time
$w(x,t)$	time depended transverse deflection of the beam
x	spatial coordinate along the length of the beam
x_{a_j}	location of the accelerometers
x_b	location of the circular brass plate
x_{r_j}	random mass locations on beam

$\dot{(\bullet)}$	derivative with respect to time
FRF	Frequency Response Function
SFEM	Stochastic Finite Element Method

List of Figures

List of Tables